National Aeronautics and Space Administration

A family of newborn planets transiting V1298 Tau

Author: Trevor J. David (3262)
Eric E. Mamajek (3260), Gautam Vasisht (3262)

Introduction

Planet properties evolve with time, and this evolution is particularly dramatic at small orbital separations. Radii shrink and temperatures drop as planets cool and contract. Eccentric orbits circularize under the influence of stellar tidal potentials. Atmospheres may erode from exposure to intense stellar emission at X-ray and extreme UV wavelengths. Theoretical models predict that the radii of *Kepler*-type planets (periods < 100 days, radii < 4 $R_\oplus$) are several times larger at ages of a few to tens of million years (Owen & Wu 2013). **While there is no shortage of theoretical predictions, there is a serious dearth of planets known around young stars.** Consequently, each young exoplanet is a rare and valuable benchmark with which theoretical planet evolution models can be tested. Transiting planets are particularly valuable, allowing for precise determinations of the planet's mass, radius, temperature, eccentricity, and orbital alignment with the stellar rotation. Furthermore, the atmospheres of transiting planets can be studied in detail through transmission spectroscopy.

Methodology

Kepler, in its extended *K2* mission, targeted fields near the ecliptic plane including thousands of stars belonging to young stellar populations (ages 1-1000 Myr). Using spatio-kinematic information from *Gaia*, we searched the entire *K2* source catalog for candidate members to young stellar populations and identified ~2900 such stars. Among those are 432 candidate members of the Taurus-Aurigae star-forming region (<5 Myr; 140 pc). We performed a systematic search for transiting planets within the *K2* light curves for the Taurus-Aurigae stars, finding a single transiting planet host: V1298 Tau.

Although several groups previously searched these light curves, the planets of V1298 Tau were not found likely because of the stellar variability. **Typical young stars may vary in brightness by several percent over timescales of hours to days, presenting a challenge to standard "de-trending" procedures.** We employed a flexible spline fit with iterative outlier rejection to pre-condition light curves for a box-least-squares transit search. After the initial detection stage, we then simultaneously modeled the stellar variability and planetary transits using a Gaussian process and analytic transit models (Figure 1). This procedure naturally accounts for the uncertainty in the planetary radii introduced by the unknown slope of stellar variability in transit.

Table 1.

	Planet c	Planet b	Planet d
Period (days)	8.2480	24.1386	>36
Radius ($R_\oplus$)	5.9 ± 0.3	10.2 ± 0.6	10.4 ± 0.9

Results

We detect three transiting planets around V1298 Tau (David et al. 2019). A detailed membership analysis reveals that V1298 Tau is not a member of the star-forming clouds in Taurus, but a separate population named Group 29, which was only recently discovered from *Gaia* (Oh et al. 2017). Group 29 has an age between 20-30 Myr (Luhman 2018), **making V1298 Tau the first pre-main sequence star to host multiple transiting planets.**

The radii of all three planets are between the size of Neptune and Jupiter (Table 1), much larger than typical close-in planets (<4 $R_\oplus$) found by *Kepler* (Figure 2). For context, there is only one other star known to host three planets larger 5 $R_\oplus$ at such small separations: the touchstone system Kepler-51, which hosts unusually low-density planets. Radial velocities indicate a 3σ upper limit to the mass of the middle planet of <0.9 M_{Jup} (Beichman et al., submitted). It is likely that the planets orbiting V1298 Tau will contract significantly over the next ~Gyr. The system may thus represent a progenitor to the compact, multi-planet systems found in great numbers by *Kepler*.

Conclusions

1. We report the detection of three large planets transiting the 20-30 million-year-old star V1298 Tau, which are among the youngest ever discovered.
2. Though the planets are large (between the size of Neptune and Jupiter), they are unlikely to be as massive as Jupiter. Instead, V1298 Tau likely represents a progenitor of the compact, multi-planet systems found in great numbers by the *Kepler* mission.
3. The inner planet is expected to be actively losing mass through photo-evaporation. The outer planets should be largely shielded from the effects of photo-evaporation, and thus may tell us about the initial conditions of typical *Kepler* planets.

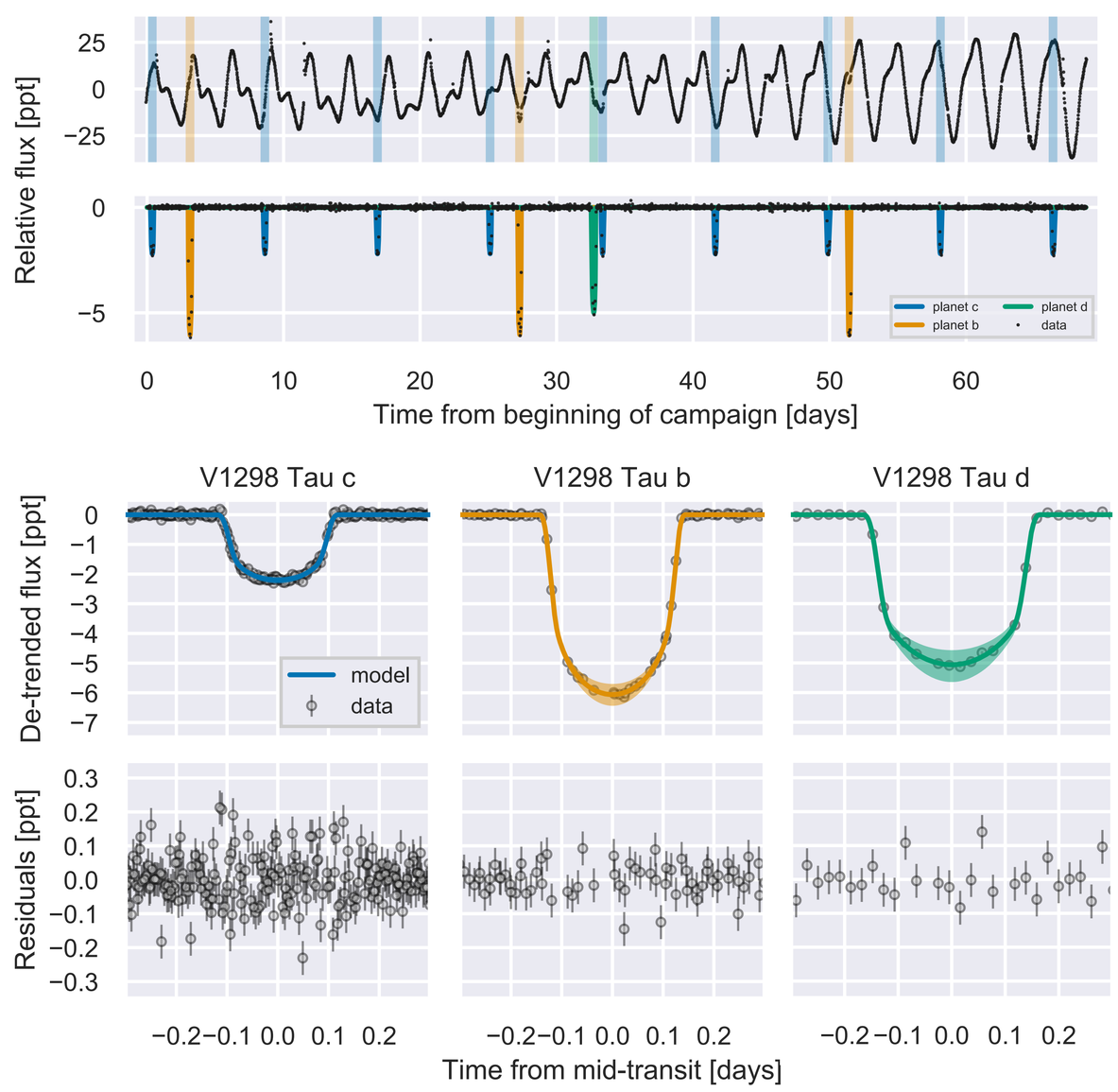

Figure 1. *K2 light curve of V1298 Tau before and after subtraction of the GP model (top two panels). Quasi-periodic brightness modulations with a period of 2.86 days are due to rotation of the star's spotted surface. Phase-folded transit data (points), mean transit models (solid lines) and their 1-σ contours (shaded bands) are shown in the third row. Below, residuals from the mean transit model.*

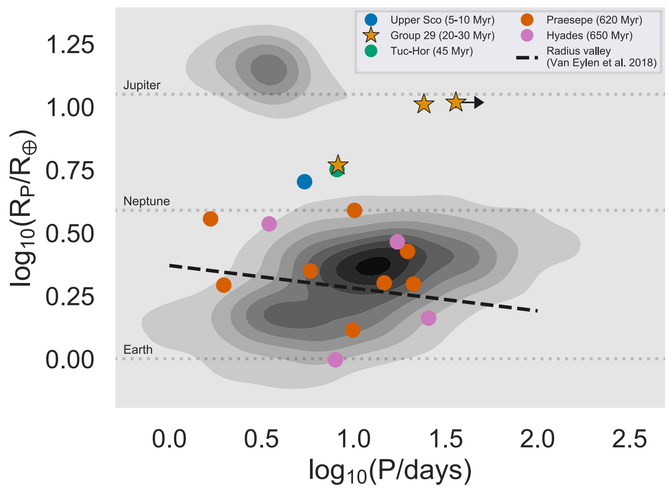

Figure 2. *Contours show a kernel density estimate of known transiting exoplanets in the orbital period vs. radius plane. Many of the youngest known planets reside in low occurrence regions of this parameter space, while some are indistinguishable from the global population.*

References

David et al., arXiv:1902.09670
Luhman, 2018, *AJ*, 156, 271
Oh et al. 2017, *AJ*, 153, 257
Owen & Wu, 2013, *ApJ*, 775, 105

National Aeronautics and Space Administration
Jet Propulsion Laboratory
California Institute of Technology
Pasadena, California

www.nasa.gov

Poster No. A-01

From scattered-light to millimeter emission: A global view of the Gyr-old system of HD 202628 and its eccentric debris disk

Virginie Faramaz[1], John Krist[1], Karl Stapelfeldt[1], Geoffrey Bryden[1]

[1]Jet Propulsion Laboratory, California Institute of Technology, Pasadena, CA, United States

Debris disks contain solid bodies in collisional cascade, ranging from km-sized down to micron-sized dust grains. They are remainders of planetary formation processes.
As example, our own Solar system hosts the Main Asteroid and the Kuiper belts, which shape and extent is driven by interactions with planets.
Consequently, extrasolar debris disks can provide crucial information on the planetary content of a system, especially in systems where planets are expected too far out to be detectable through radial velocities of transit techniques and in systems too old for planets to be directly imaged.

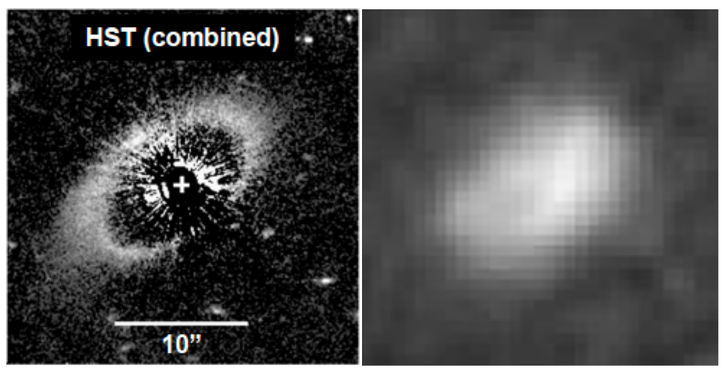

Left: *HST*/STIS coronagraph images of the HD 202628 disk (combined observations of Krist+ 2012 & Schneider+ 2016). **Right:** *Herschel*/PACS 70 microns observation, that shows a characteristic pericenter-glow expected from eccentric debris disks (Wyatt+ 1999)

- HD 202628 is a Gyr-old Solar-type star surrounded by an eccentric debris disk unraveled by HST in 2011. It therefore hosts a belt-shaping (and yet invisible) planet on an eccentric orbit.
- As eccentric planets have been found to be much more common than the sole study of the Solar System hinted at, HD 202628 is probably a much more representative mature exoplanetary system than the Solar System is.

- From the study of the disk seen in scattered light with HST, the belt-shaping companion should have a maximum mass of ~15 M_{Jup} and orbit at a minimum separation ~ 3".
- It is thus not possible to characterize it via Radial Velocities or Transit techniques, and current direct imaging capabilities do not allow the observation of such a companion around a star as old as HD 202628.

CHARACTERIZING THE ECCENTRIC DISTANT COMPANION RELIES ON CHARACTERIZATION OF ITS GRAVITATIONAL IMPRINT ON THE BELT AND ACCURATE KNOWLEDGE OF ITS GEOMETRY

This can be achieved thanks to ALMA high resolution observations at millimeter wavelengths, as these wavelengths probe much larger grains that HST does, which are much less affected by stellar radiation effects, and which spatial distribution bears therefore more clearly the gravitational imprint of the companion

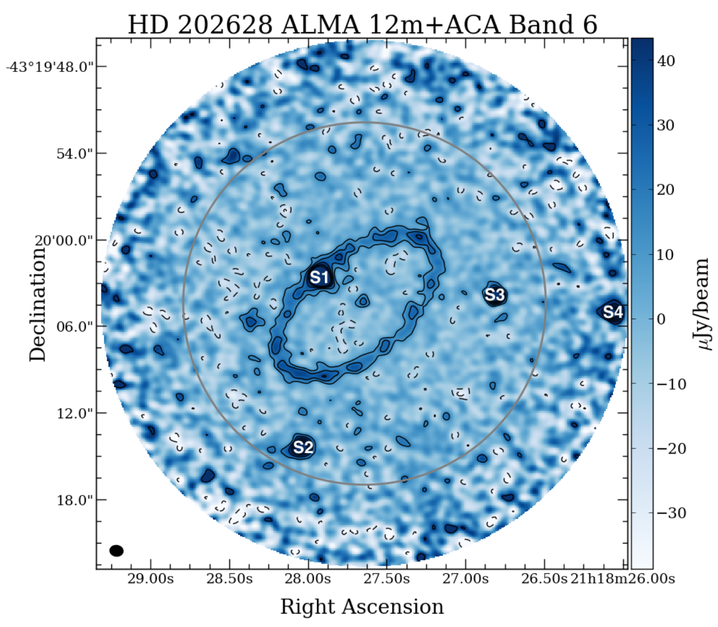

Parameter	Value
M_{disk} ($M_\oplus$)	$(1.36 \pm 0.06) \times 10^{-2}$
Inner radius (AU)	143.1 ± 1.7
Outer radius (AU)	165.5 ± 1.4
Inclination (°)	57.4 ± 0.4
PA (°)	$-50.4^{+0.4}_{-0.5}$
Eccentricity	$0.09^{+0.02}_{-0.01}$

Left: ALMA 1.3 mm continuum observations of HD 202628 (PI= V. Faramaz). Contours show the 2, 4, 6,... σ significance levels, with σ = 5.4 Jy/beam. The resolution of this map is ~0".8. The stellar photosphere appears inner to the ring and is detected with SNR 5. It is offset from the ring center of symmetry, which confirms the intrinsic eccentricity of the debris belt. Bright sources (SNR> 6) within the field are labeled from S1 to S4. **Right:** Result of the MCMC fit on the ring geometry as found by ALMA.

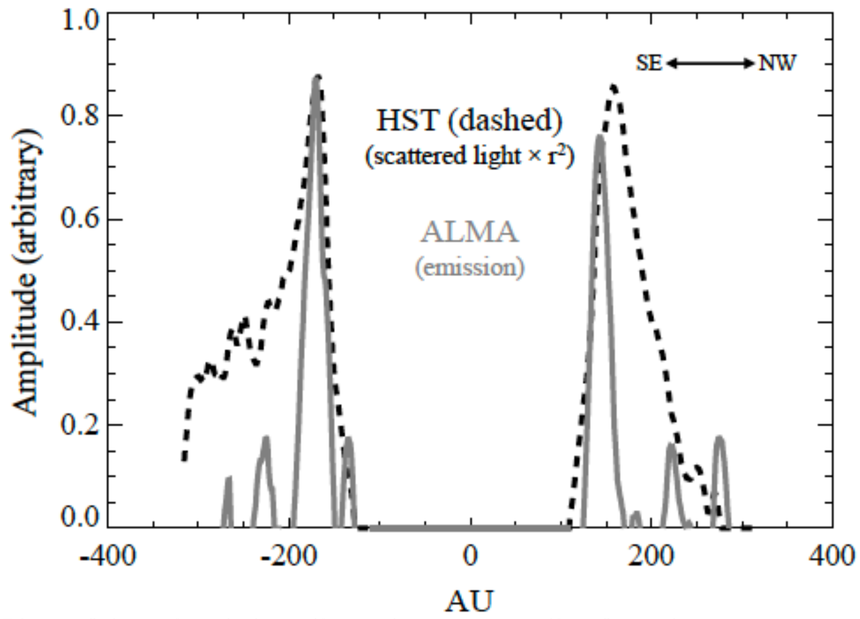

Plots of the azimuthal median value versus radius from the star measured in 36º sectors aligned along the line of nodes of the deprojected HD 202628 HST relative density map (dashed line) and the deprojected ALMA image.

- HST and ALMA data agree on the position of the ring inner edge, however, the ring is much narrower seen with ALMA than with HST. With R=143.8 AU and ΔR≈ 20 AU, $\Delta R/R < 0.5$, and hence, this debris disk pertains to the class of narrow rings (along with Fomalhaut and HR4796, Hughes+ 2018).
- This type of narrow ring has been suggested to originate from collisions between irregular satellites surrounding a belt-shaping planet (Hayakawa & Hansen, in prep), which is extremely interesting in this context as we suspect the source S1 to be circumplanetary material surrounding the expected companion.
- The status of this source will be soon ascertained with new ALMA observations (PI= V. Faramaz) that will determine whether S1 is comoving with the star or not.
- If this source proves to be comoving with the star, it would be the very first time circumplanetary material is directly observed and would provide a target of choice for future JWST observations.

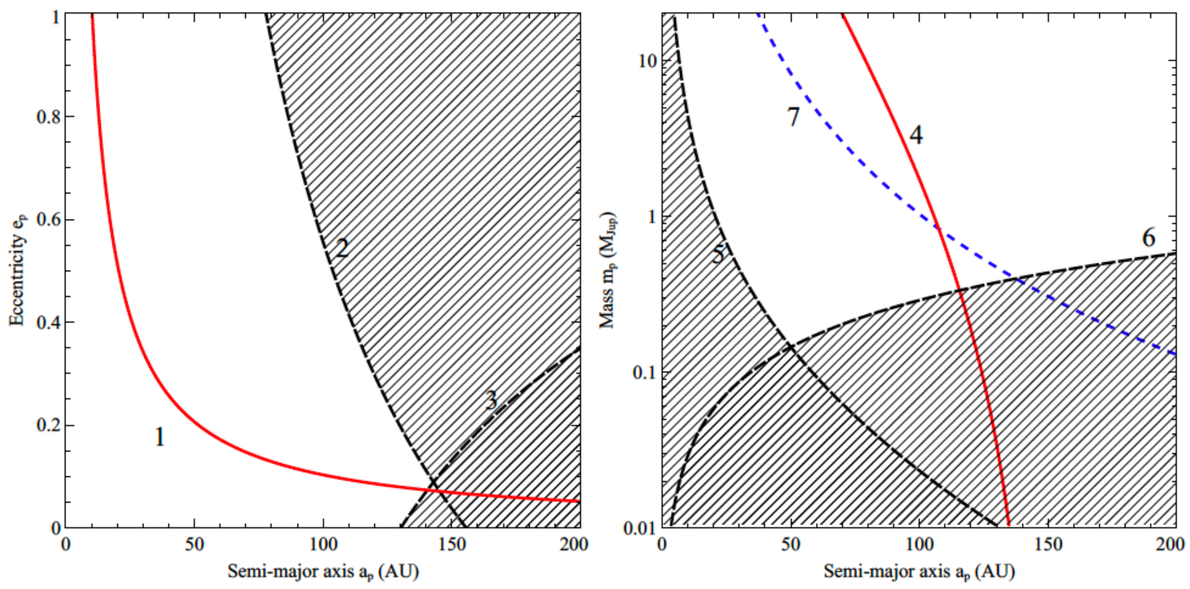

Theoretical constraints on the belt-shaping eccentric perturber (mass, semimajor axis, eccentricity) :

- (1) The eccentricity imposed on the ring is 0.09.
- (2) and (3) : The apastron and periastron of the planet should not cross the ring.
- (4) The planet should carve the inner edge at 143.1 AU.
- The mass of the planet should be such that the dynamical timescales allow it to (5) empty its surroundings and carve the inner edge and (6) give the ring its eccentric shape.
- (7) : couples (a_p,m_p) that correspond to a Hill radius compatible with the half extent of the sources S1. If S1 were indeed circumplanetary material surrounding the belt-shaping planet, and under the assumption that the material fills the planet's Hill radius, one would be able to fully characterize it, alleviating degeneracies between the mass and orbital parameters.

References: Krist et al. 2012, AJ, 144, 45 • Schneider et al. 2016, AJ, 152, 64 • Wyatt et al. 1999, ApJ, 527, 918 • Hughes et al. 2018, ARA&A, 56, 541 • Hayakawa & Hansen (in prep)

Poster No. A-02

National Aeronautics and Space Administration

The surprising scattering properties of the HR 4796 A debris disk

Johan Mazoyer (3262, NASA Sagan Fellow)

C. Chen (STScI), B. Ren (JHU), G. Duchene (UC Berkeley), P. Arriaga (UCLA), M. Millar-Blanchaer (3262), B. Mennesson (3262) & GPI LLP collaboration

HR 4796 A is a close-by young star which harbors a debris disk first imaged in scattered light in 1999. Its narrow and sharply carved belt at 80 AU made it a very popular target for all imaging instruments from the visible to the far IR since then, constraining further its geometrical parameters and spatial extension. Measurements of scattered light phase functions have long been used as a powerful tool to measure dust grain properties of comets and asteroids in the solar system.

For exosolar debris disks, in-situ measurements are impossible; therefore, high-contrast imaging observations in visible and near-IR are needed to infer the dust properties. They have been extracted for only a few disks so far. Indeed, extraction of these observables is complicated by the PSF subtraction techniques applied to coronagraphic images, whose effects have to be carefully corrected. We have recently obtained observations of this debris disk with Gemini/GPI. This scattering phase function is different from ones not only measured on the limited sample of debris disks but also on various dust populations in the solar system. Using this observable, we use MCFOST, a radiative transfer code to constrain the dust properties for this object.

GEOMETRICAL ANALYSIS

Geometrical analysis using 4 different reduction techniques showed consistent results :

- KLIP ADI [1]
- Mask & Interpolate [2]
- NMF [3]
- KLIP RDI [1]

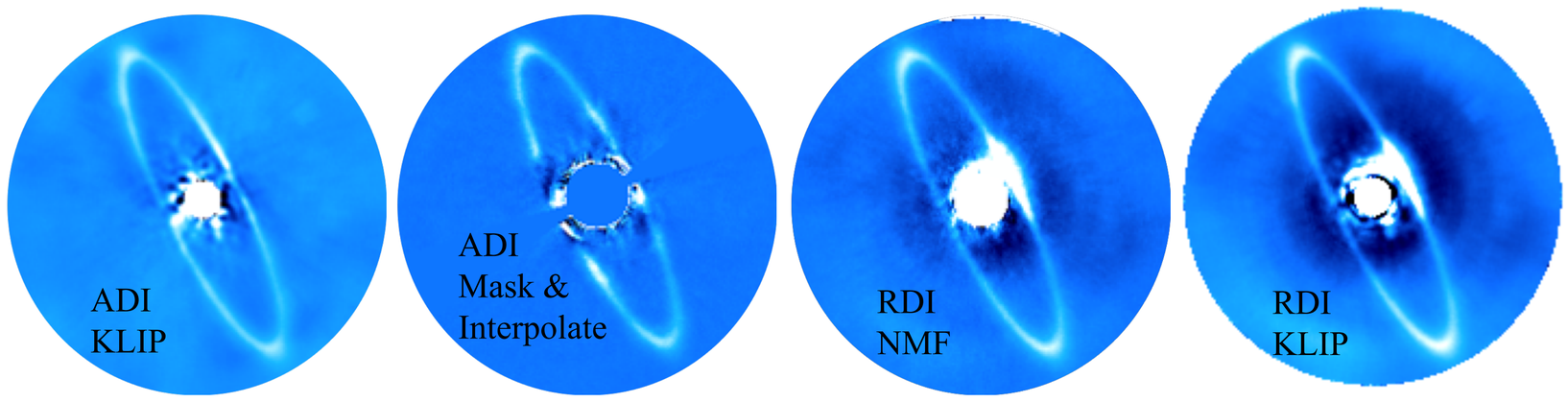

MCMC ANALYSIS

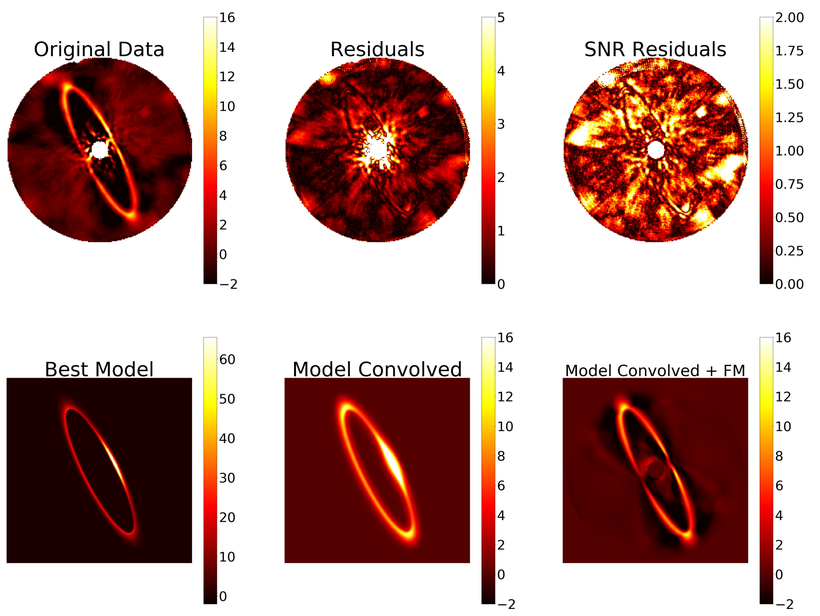

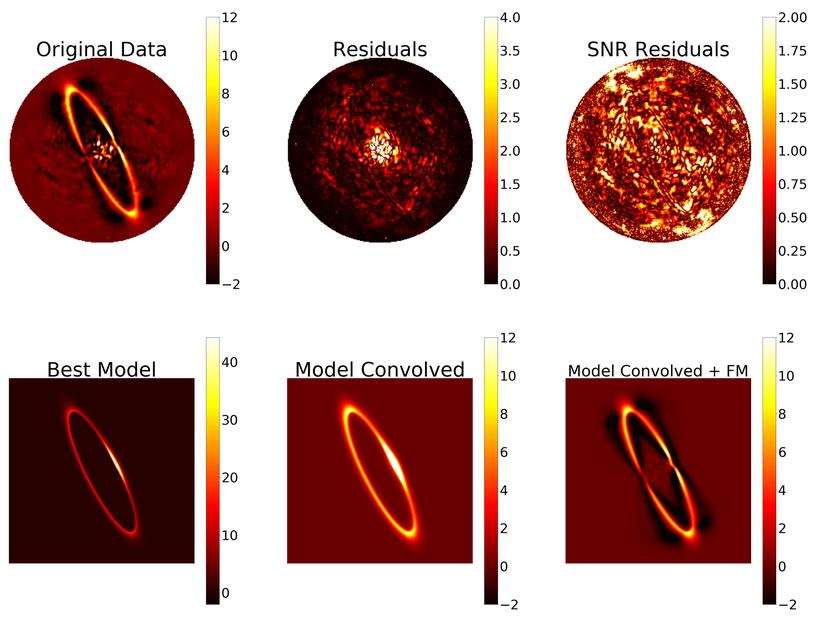

Markov Chain Monte Carlo analysis on all the data using a forward modeling approach to correct for the bias introduced by the ADI [4].

Geometrical parameters extracted 2 component Henyey-Greenstein to fit the scattering phase functions.

We also analyzed SPHERE data already published by Milli+ 2017 [5] for comparison.

SCATTERING PHASE FUNCTIONS

HR 4796 scattering phase function (SPF) is different from the ones measured not only on the limited sample of debris disks but also on different dust population in the solar system [6], with (1) an extremely forward scattering curve, (2) a dip at scattering angles from 30° to 70° (the SPF minimum is usually around a 90°), and (3) a rise at high scattering angles.

We find an SPF close but significantly different than [5]. We tried more complicated mathematical functions (3 component Henyey-Greenstein) with the same result.

All spectral bands (J H K1 K2) show the same SPF: predicted differences between them are smaller than our error bars.

We used a radiative transfert code MCFOS [7]. A large minimum grain size was required to reproduce the observed back scattering from the back side of the disk (expected from an active A star).

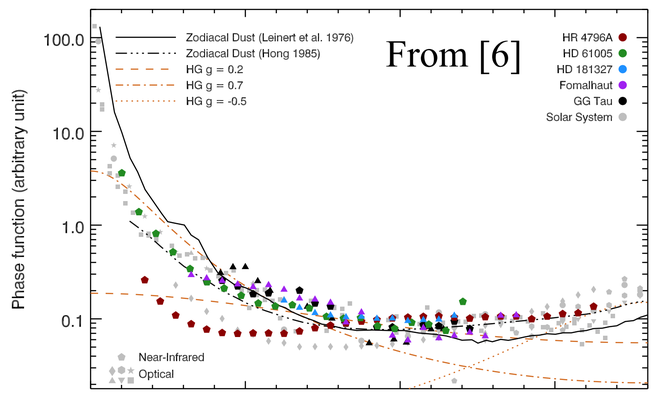

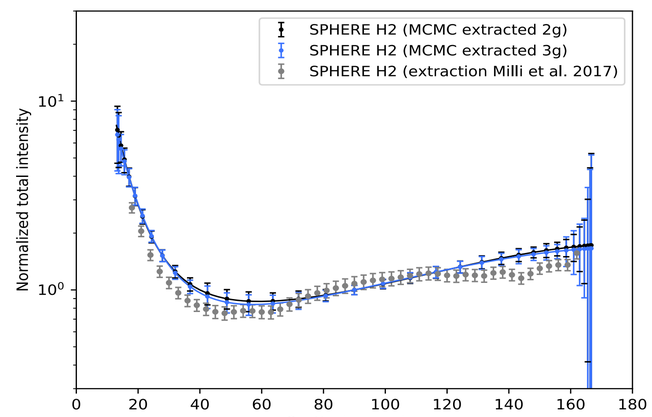

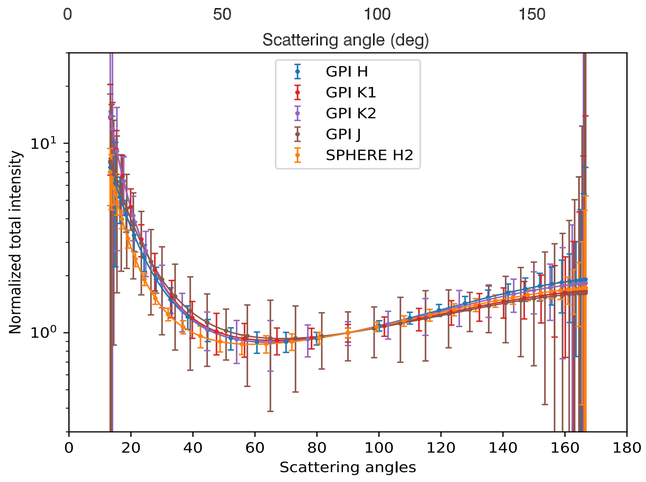

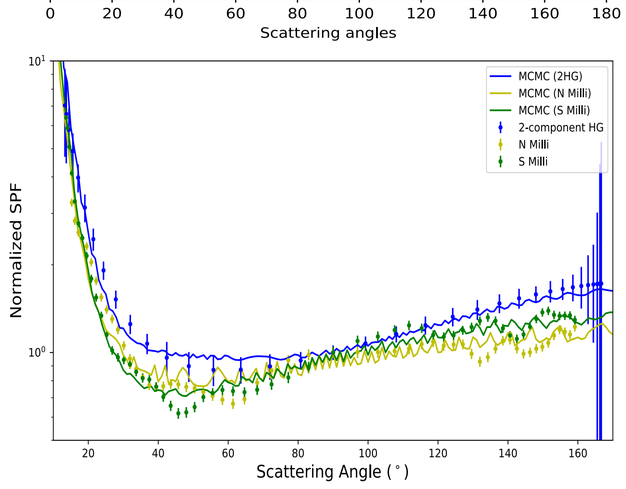

References:

[1] Soummer et al. 2012 ApJ
[2] Perrin et al. 2015 ApJ
[3] Ren et al. 2018 ApJ
[4] Pueyo 2016 ApJ
[5] Milli et al. 2017 A&A
[6] Hughes et al. 2018 ARAA
[7] Pinte et al. 2006 A&A

National Aeronautics and Space Administration

Jet Propulsion Laboratory
California Institute of Technology
Pasadena, California

www.nasa.gov

Poster No. A-03

National Aeronautics and Space Administration

Neighbor bias: an understudied observational systematic in galaxy surveys

Author: Albert Izard (3266)
Co-Authors: Alina Kiessling (3266), Eric Huff (3268)

Dark energy experiments in the 2020s will be systematics-limited unless all significant sources of errors are identified and well understood.
We developed a model for the neighbor bias, a general class of observational systematics that can produce percent-level biases.
We provide a mitigation strategy for an optimal extraction of cosmological information.

Problem

- NASA's Wide-Field Infrared Survey Telescope (WFIRST) and the ESA/NASA Euclid telescope are dark energy experiments that will be launched in the 2020s and will conduct imaging galaxy surveys. They will probe the dark matter distribution by analyzing the galaxy positions (galaxy clustering) and the galaxy shapes (weak lensing).
- Detecting a galaxy and measuring its shape accurately is harder in the presence of nearby galaxies. This **neighbor bias** can be sourced by (see figure):
  - The light contamination from neighbors.
  - The overlap of multiple galaxies into a single blended blob.
  - The presence of faint and undetected galaxies.
  - The amount of background light.
  - The obscuration from extended sources reducing the detection efficiency.

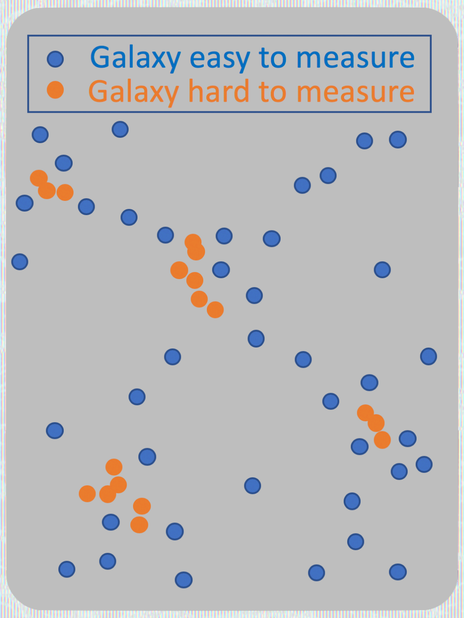

- **Unresolved questions**:
  What is the impact of a systematic with spatial variations coupled to the signal? Can we ignore the neighbor bias in Euclid and WFIRST? How can it be mitigated? There is a lack of methods addressing these questions.

Methodology

- We developed efficient numerical techniques to simulate galaxy formation and the large-scale structure across cosmic times.
- We built an **analytical model for the neighbor bias**. We showed that a wide variety of systematic errors are well explained by a linear coupling with the matter density field, as shown in the figure.

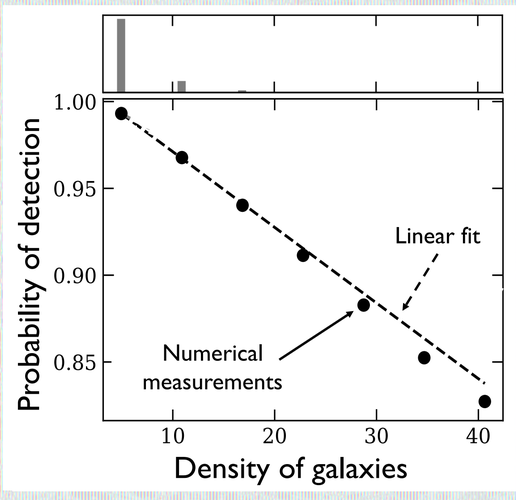

Histogram of the sky map cell's density (high occupancy of a cell is rare).

Linear coupling in our model between the error and the local density of galaxies on the sky.

- The model provides predictions of the biases on the measurements of galaxy clustering and weak lensing.
- To test the model, we use the simulated catalogs to determine numerically the impact of the neighbor bias on the observables and compare it with the model predictions.

Results

- The analytical model for the neighbor bias has a **single parameter Γ** (for each galaxy sample) that tunes the strength of the coupling: $\text{Error} = \Gamma\delta$
- We find biases in the observables at the percent level that are scale independent for galaxy clustering but show scale dependence for weak lensing (see fig.)

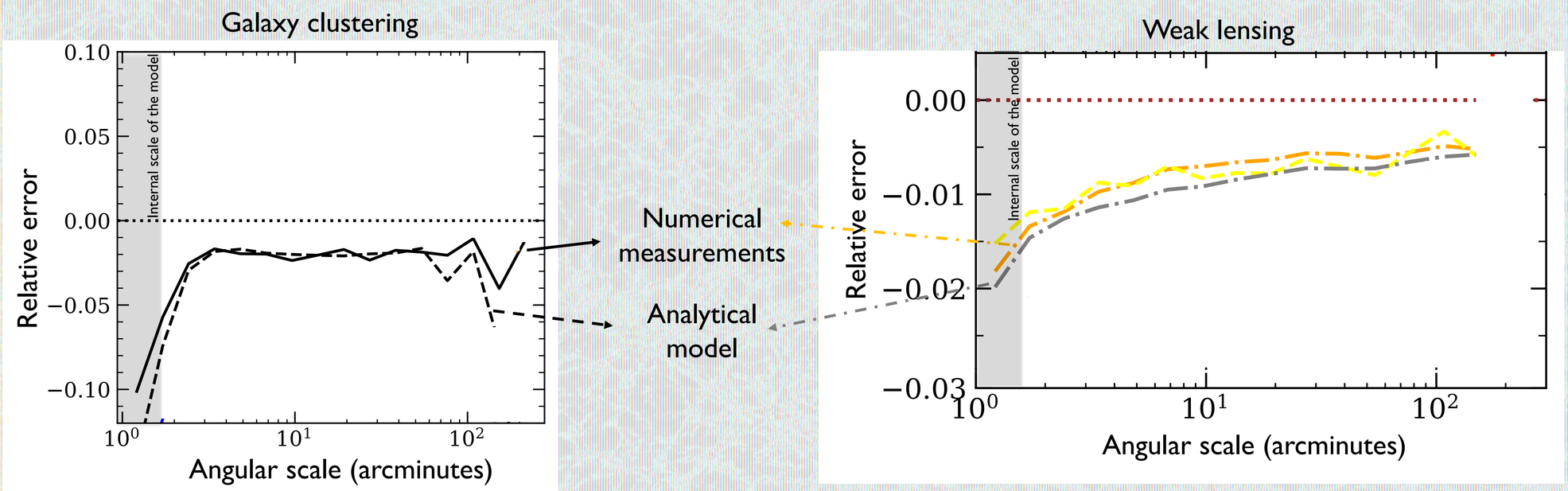

Galaxy clustering and weak lensing measure the excess of structure with respect to a random spatial distribution. The neighbor bias produces biases at the percent-level for such observables. The model predictions agree with the numerical measurements.

- Such errors are mostly unaccounted for in current analysis and will compromise the results of future and more precise surveys as WFIRST and Euclid. We suggest that a strategy to **mitigate** all the possible channels of neighbor bias is to encapsulate them all in our analytical model, which has to be plugged in into the software for model fitting to the data, and to marginalize over the added nuisance parameters.

Benefit to JPL

- The techniques presented here enable JPL to efficiently produce simulated extra-galactic catalogs with many layers of realism and identify new systematic errors.
- This work puts JPL in the forefront of mitigating observational systematics affecting the observables of WFIRST and Euclid.

National Aeronautics and Space Administration
Jet Propulsion Laboratory
California Institute of Technology
Pasadena, California

www.nasa.gov

Background image from the simulations used in this project

Poster No. A-05

National Aeronautics and Space Administration

Neighbor bias: an understudied observational systematic in galaxy surveys

Author: Albert Izard (3266)
Co-Authors: Alina Kiessling (3266), Eric Huff (3268)

Dark energy experiments in the 2020s will be systematics-limited unless all significant sources of errors are identified and well understood.
We developed a model for the neighbor bias, a general class of observational systematics that can produce percent-level biases.
We provide a mitigation strategy for an optimal extraction of cosmological information.

Problem

- NASA's Wide-Field Infrared Survey Telescope (WFIRST) and the ESA/NASA Euclid telescope are dark energy experiments that will be launched in the 2020s and will conduct imaging galaxy surveys. They will probe the dark matter distribution by analyzing the galaxy positions (galaxy clustering) and the galaxy shapes (weak lensing).
- Detecting a galaxy and measuring its shape accurately is harder in the presence of nearby galaxies. This **neighbor bias** can be sourced by (see figure):
  - The light contamination from neighbors.
  - The overlap of multiple galaxies into a single blended blob.
  - The presence of faint and undetected galaxies.
  - The amount of background light.
  - The obscuration from extended sources reducing the detection efficiency.

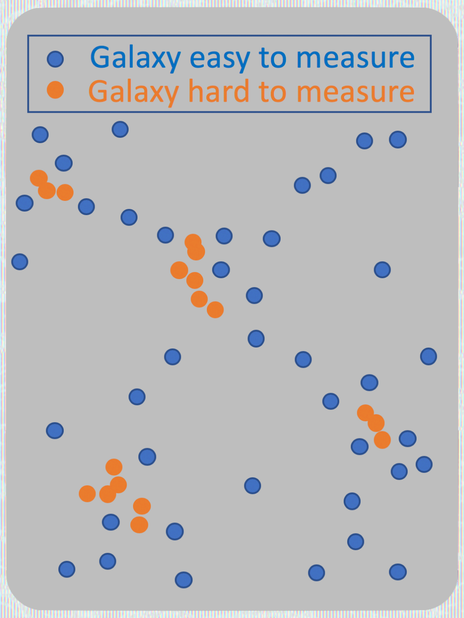

- **Unresolved questions**:
  What is the impact of a systematic with spatial variations coupled to the signal? Can we ignore the neighbor bias in Euclid and WFIRST? How can it be mitigated? There is a lack of methods addressing these questions.

Methodology

- We developed efficient numerical techniques to simulate galaxy formation and the large-scale structure across cosmic times.
- We built an **analytical model for the neighbor bias**. We showed that a wide variety of systematic errors are well explained by a linear coupling with the matter density field, as shown in the figure.

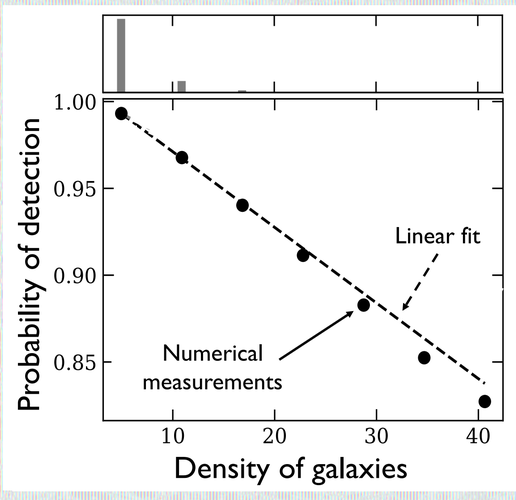

Histogram of the sky map cell's density (high occupancy of a cell is rare).

Linear coupling in our model between the error and the local density of galaxies on the sky.

- The model provides predictions of the biases on the measurements of galaxy clustering and weak lensing.
- To test the model, we use the simulated catalogs to determine numerically the impact of the neighbor bias on the observables and compare it with the model predictions.

Results

- The analytical model for the neighbor bias has a **single parameter Γ** (for each galaxy sample) that tunes the strength of the coupling: $\text{Error} = \Gamma\delta$
- We find biases in the observables at the percent level that are scale independent for galaxy clustering but show scale dependence for weak lensing (see fig.)

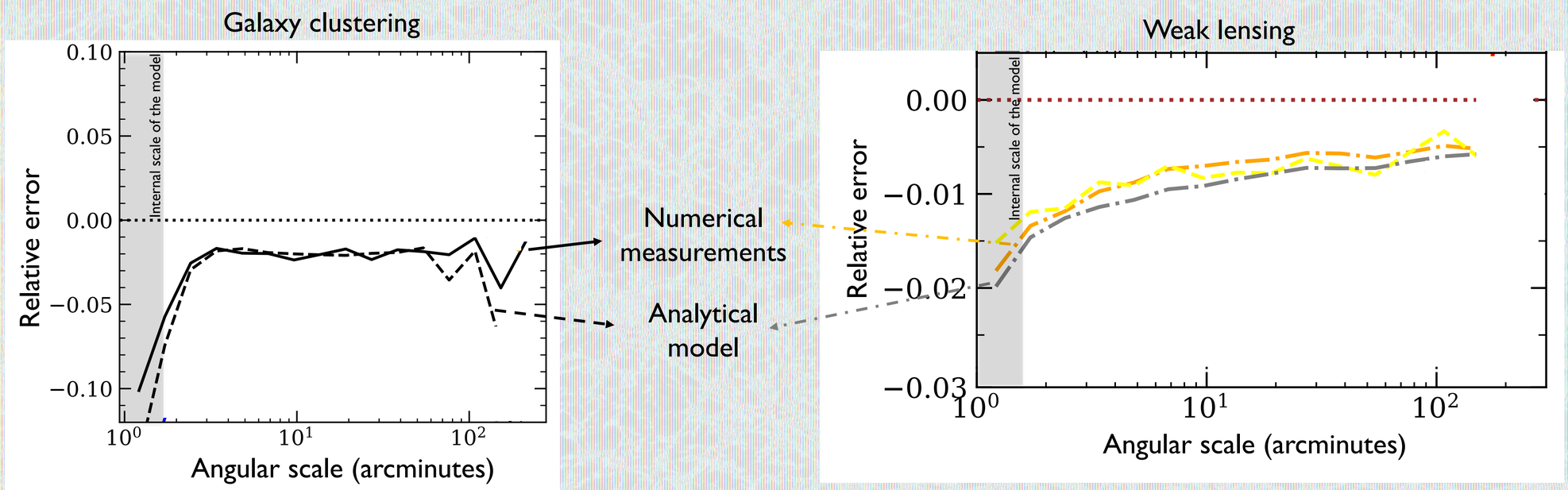

Galaxy clustering and weak lensing measure the excess of structure with respect to a random spatial distribution. The neighbor bias produces biases at the percent-level for such observables. The model predictions agree with the numerical measurements.

- Such errors are mostly unaccounted for in current analysis and will compromise the results of future and more precise surveys as WFIRST and Euclid. We suggest that a strategy to **mitigate** all the possible channels of neighbor bias is to encapsulate them all in our analytical model, which has to be plugged in into the software for model fitting to the data, and to marginalize over the added nuisance parameters.

Benefit to JPL

- The techniques presented here enable JPL to efficiently produce simulated extra-galactic catalogs with many layers of realism and identify new systematic errors.
- This work puts JPL in the forefront of mitigating observational systematics affecting the observables of WFIRST and Euclid.

Background image from the simulations used in this project

National Aeronautics and Space Administration
Jet Propulsion Laboratory
California Institute of Technology
Pasadena, California

www.nasa.gov

Poster No. A-05

National Aeronautics and Space Administration

CWISEP J193518.59-154620.3: an extremely cold brown dwarf in the Solar neighborhood discovered with CatWISE

Author: Federico Marocco (3266)

Dan Caselden (Gigamon ATR), Aaron Meisner (NOAO), J. Davy Kirkpatrick (IPAC), Edward L. Wright (UCLA), Jacqueline K. Faherty (AMNH), Christopher R. Gelino (IPAC), Peter R. Eisenhardt (JPL/3266), John W. Fowler (IPAC), Michael C. Cushing (U. Toledo), Roc M. Cutri (IPAC), Nelson Garcia (IPAC), Thomas H. Jarrett (U. Cape Town), Renata Koontz (UCR), Amanda Mainzer (JPL/3266), Elijah J. Marchese (UCR), Bahram Mobasher (UCR), David J. Schlegel (LBNL), Daniel Stern (JPL/3266), Harry I. Teplitz (IPAC)

1

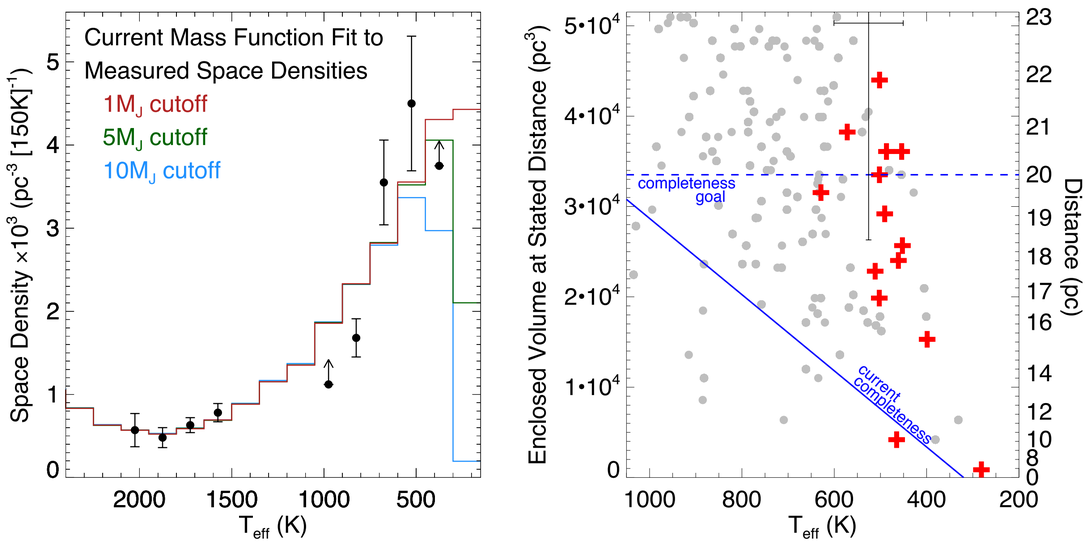

The census of objects in the Solar neighborhood is still incomplete. Extremely cold sub-stellar objects (known as brown dwarfs; Kumar 1962) are challenging to identify, even in close proximity to us, because of their intrinsic faintness. Kirkpatrick et al. (2019) found that the Solar neighborhood census completeness limit drops to less than 8 pc (~26 light years) for objects as cold as 300 K (right panel). This incompleteness has prevented us from answering one of the most fundamental questions in all of astrophysics – how star formation can create objects of extremely low mass, and the efficiency with which it does so. Preliminary results from Kirkpatrick et al. (2019) show that the cutoff mass for star formation must be lower than 10 M_{Jup} because the model predictions for such a cutoff are underpredicting the observed space density (left panel).

2

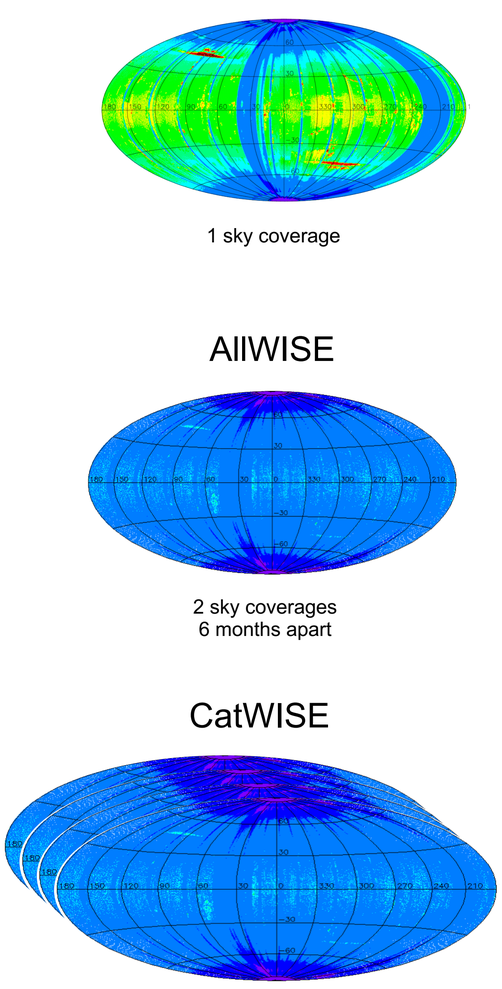

Finding more of these cold nearby objects is one of the goals of CatWISE, a NASA ADAP funded project that combined data from the 2010-2016 phases of NASA's WISE and NEOWISE mission (Wright et al. 2010, Mainzer et al. 2014). CatWISE has produced a catalog of ~900 million sources with measured W1 (3.4 μm) and W2 (4.6 μm) photometry, and motion. CatWISE is built over 4x more data than its predecessor, AllWISE (Cutri et al. 2013) covering the full sky 8+ times over a total time baseline of 6+ years. Leveraging on this larger dataset and longer baseline, CatWISE is ~0.5 mag deeper and 10x more sensitive to motion than AllWISE (Eisenhardt 2019). The CatWISE Preliminary Catalog is available at catwise.github.io.

References: Cutri et al., 2013, Explanatory Supplement to the AllWISE Data Release Products; Eisenhardt, 2019, AAS Meeting #233, id.162.07; Kumar, 1962, Institute for Space Studies Report Number X-644-62-78; Kirkpatrick, et al., 2019, The Astrophysical Journal Supplement Series, Volume 240, Issue 2, article id. 19; Luhman, 2014, The Astrophysical Journal Letters, Volume 786, Issue 2, article id. L18; Mainzer, et al., 2014, The Astrophysical Journal, Volume 792, Issue 1, article id. 30; Wright, et al., 2010, The Astronomical Journal, Volume 140, Issue 6, pp. 1868-1881.

3

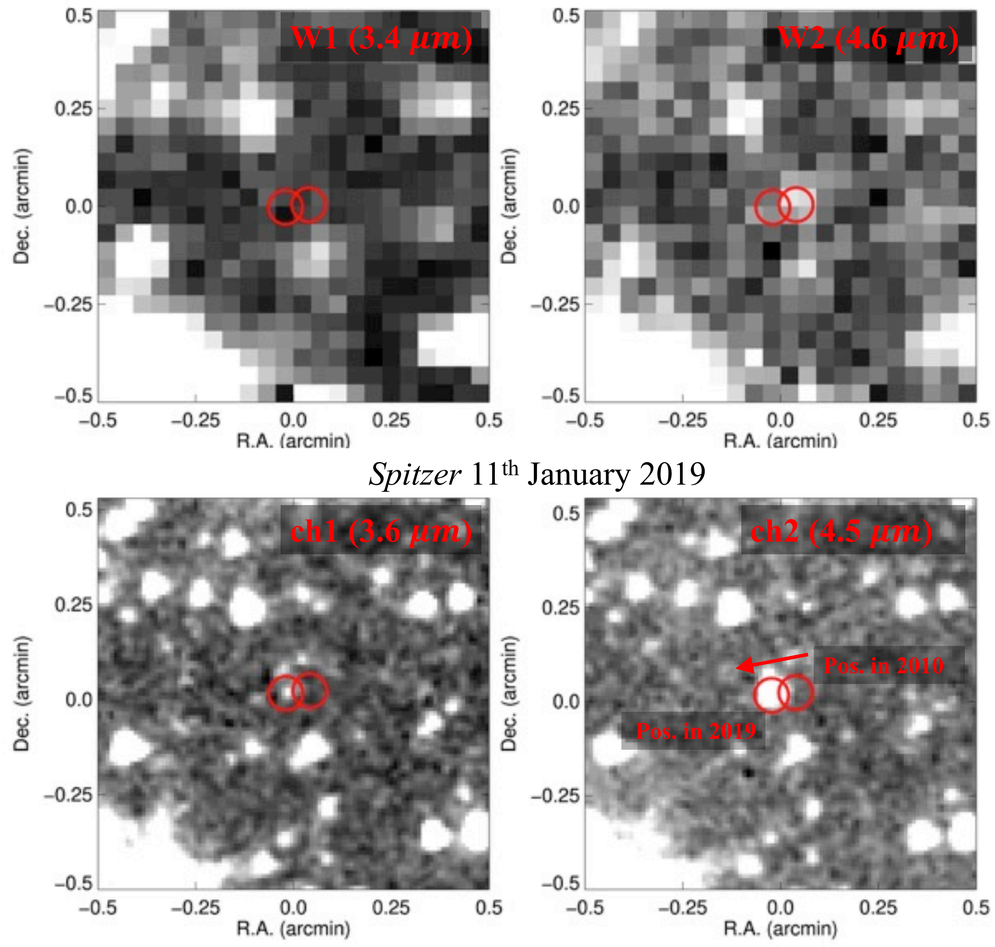

Using machine learning techniques, we selected cold brown dwarf candidates from the CatWISE Preliminary Catalog. We obtained follow-up photometry at ch1 (3.6 μm) and ch2 (4.5 μm) using NASA's *Spitzer* telescope, to confirm the nature and estimate the effective temperature of our targets. The reddest, therefore coldest object from our follow-up is CWISEP J193518.59-154620.3, with a color of ch1 − ch2 = 3.24 ± 0.31 mag. The images above show the target as seen by WISE (top row), and *Spitzer* (bottom row). The red circles mark its position at the two epochs. The motion between the two observations is clear, and we measure $\mu_\alpha \cos\delta = 337 \pm 69$ mas/yr and $\mu_\delta = -50 \pm 97$ mas/yr. The object is invisible in the W1 image, and very faint in the ch1 image, while being very bright in the W2 and ch2 images, hinting at a very cold temperature (see below).

4

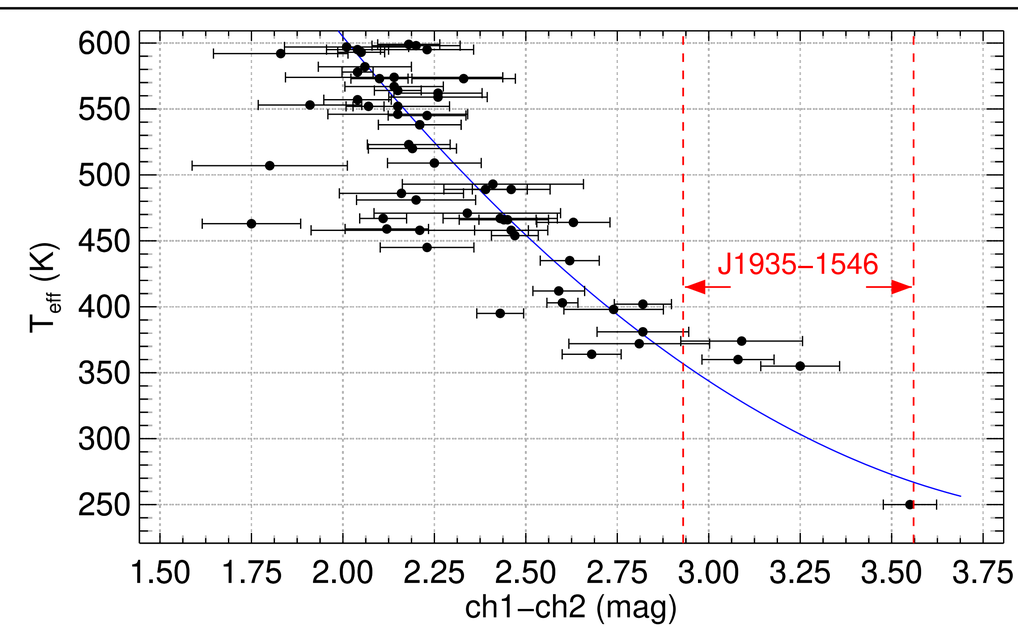

Comparing the ch1−ch2 color for CWISEP J1935-1546 with known brown dwarfs, we can see that our newly discovered object is among the reddest, therefore coldest, brown dwarfs known. Its color rivals that of the coldest brown dwarf, WISE J0855-0714 (Luhman 2014, ch1−ch2 = 3.41 mag, T_{eff} = 250 K). Using the color-temperature relation presented in Kirkpatrick et al. (2019) we derive $T_{eff} = 270 - 360$ K, which implies CWISEP J1935-1546 is at a distance of only 5.6 − 10.9 pc (18 – 35 light years).

National Aeronautics and Space Administration
Jet Propulsion Laboratory
California Institute of Technology
Pasadena, California

www.nasa.gov

Acknowledgements: This research was partly carried out at the Jet Propulsion Laboratory, California Institute of Technology, under a contract with NASA. FM is supported by an appointment to the NASA Postdoctoral Program at the Jet Propulsion Laboratory, administered by Universities Space Research Association under contract with NASA. CatWISE is funded by NASA under Proposal No. 16-ADAP16-0077 issued through the Astrophysics Data Analysis Program, and uses data from the NASA-funded WISE and NEOWISE projects. This work is based in part on observations made with the Spitzer Space Telescope, which is operated by the Jet Propulsion Laboratory, California Institute of Technology under a contract with NASA.

Poster No. A-06

National Aeronautics and Space Administration

Radiation-Pressure Waves in Black Hole Winds

Lluís Mas Ribas (3266)

Why?

Supermassive Black holes in the center of all massive galaxies can **eject the gaseous material** orbiting them.

This can **supress star formation** and even **enrich** with metals the distant intergalactic medium!

What?

a. What are the **physical processes** ejecting the material?

b. What are the **nature and properties** of this outflowing gas?

How?

Look at the **absorption signatures** of the outflows on the emission spectrum of the black hole.

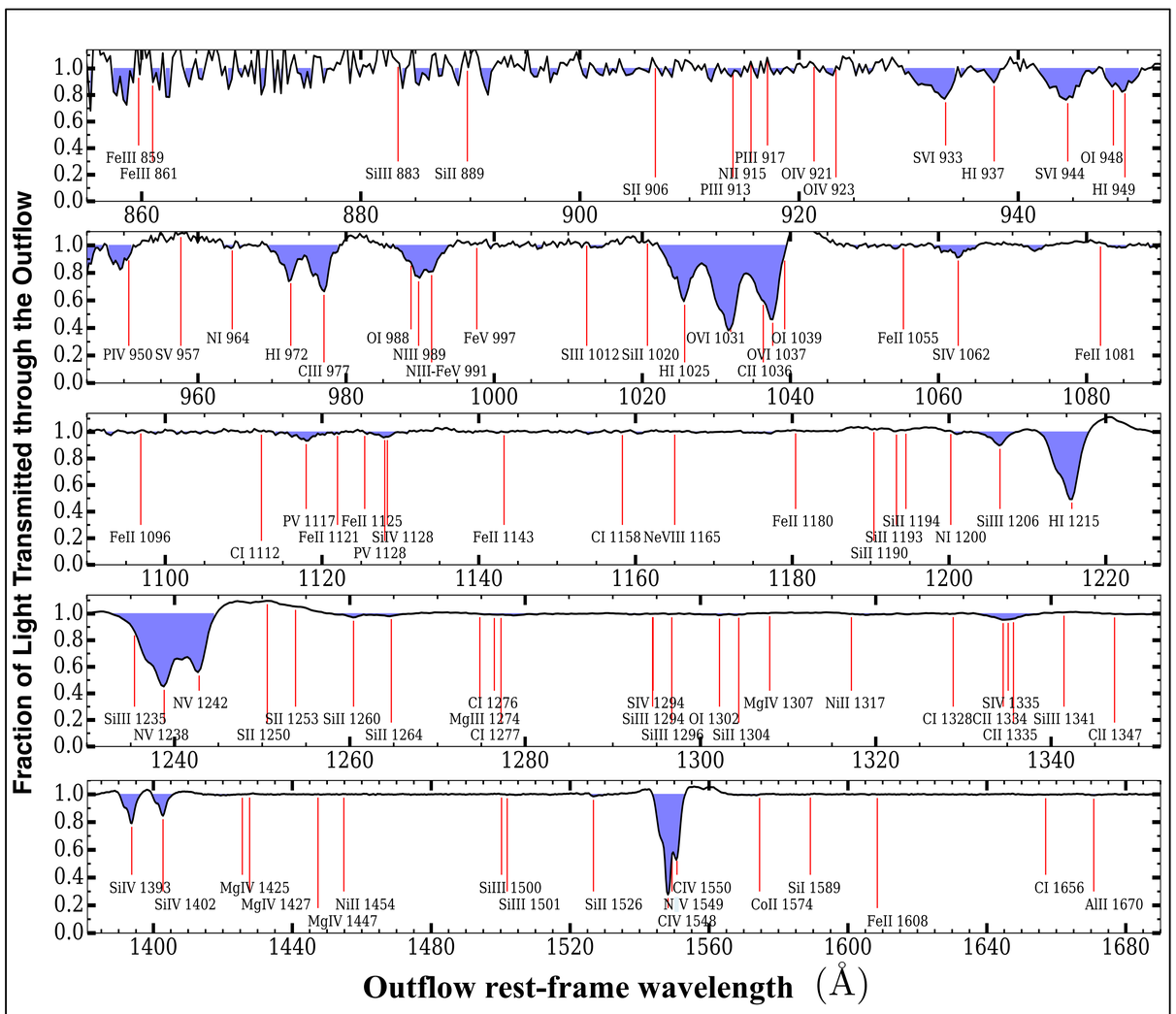

The average outflow absorption spectrum from more than 10,000 black holes (quasars) above.

* **Many metal species** in the outflows are discovered due to the stacking!

* The absorption lines denote highly-ionized hot gas, but some only exist in cold phases → It's a **Multiphase medium!**

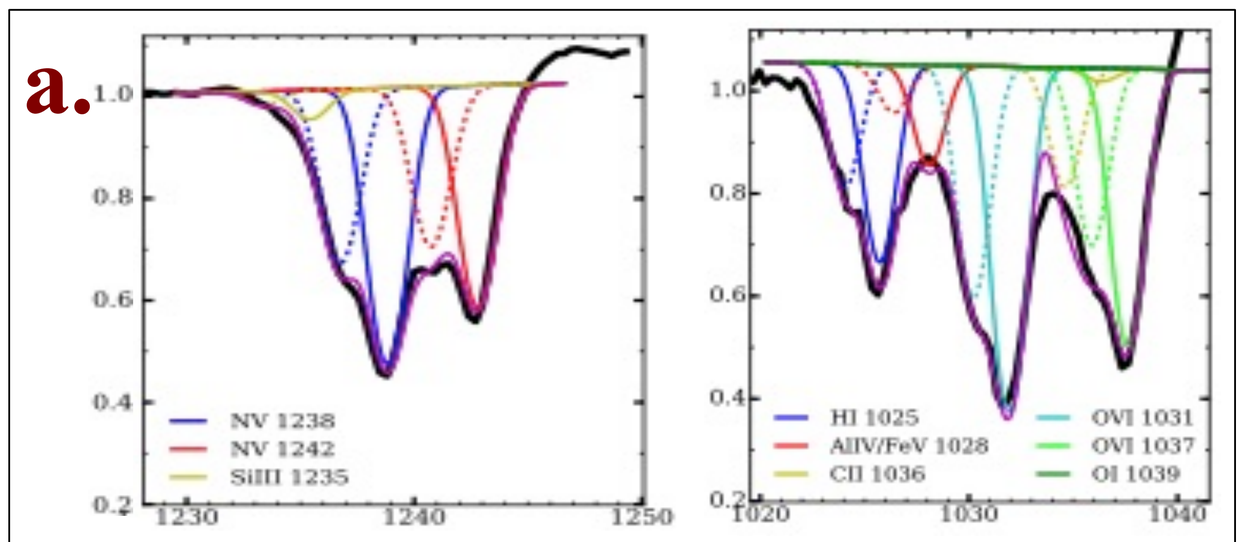

A closer look reveals that each absorption line is **actually two lines** (solid + dashed with same color) !

This only happens when it is the own **BLACK HOLE RADIATION THAT ACCELERATES THE GAS** through *line locking*, hypothesized but never conclusively seen before.

What is Line Locking?

Atoms of triply-ionized carbon (CIV) in a gas cloud absorb CIV radiation emitted from close to the black hole, and are accelerated away at a speed **v**. CIV is a doublet and thus appears as two lines.

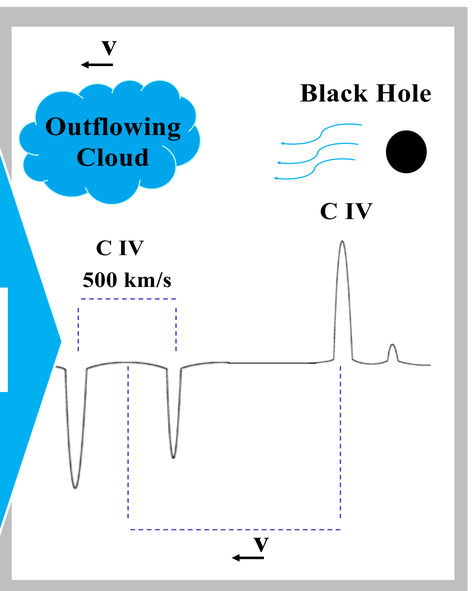

When another cloud reaches a relative velocity coinciding with the separation of the doublet, it masks radiation available for the first cloud. This effect ends up with the two clouds locked at a constant relative speed, and one extra absorption feature appearing for all metal lines.

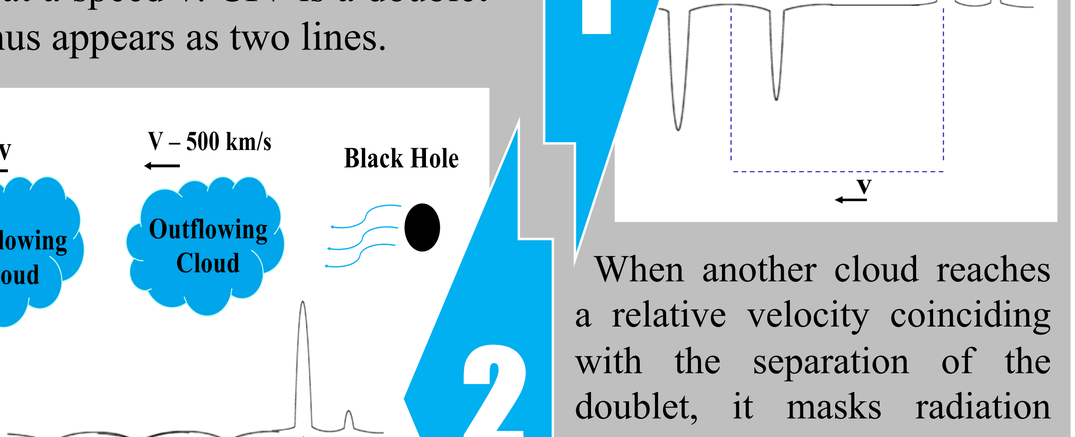

We find that **RADIATION-PRESSURE WAVES** are the best candidates to explain the multiphase structure and the acceleration. A wave scenario is consistent with modern simulations and observations of stellar winds.

National Aeronautics and Space Administration

Jet Propulsion Laboratory
California Institute of Technology
Pasadena, California

www.nasa.gov

Poster No. A-07

National Aeronautics and Space Administration

Applications of Machine Learning Techniques to Noisy Radio Data from the STO2

Author: Youngmin Seo (3266)
Paul Goldsmith (3266), Volker Tolls (CfA), Chris Walker (U. of Arizona), and STO2 team

I. INTRODUCTION

- STO2 was the first high spectral resolution terahertz balloon mission for astronomy
- 0.8-meter telescope, 50″ resolution at 158 μm
- Heterodyne receiver array for [CII] line; f = 1900.5 GHz
- Flight from Dec. 9, 2016 to Dec. 28, 2016
- ~255,000 [CII] spectra

II. CHALLENGES

- A fraction of spectral data contained features much larger than statistical noise and required a new method to process them

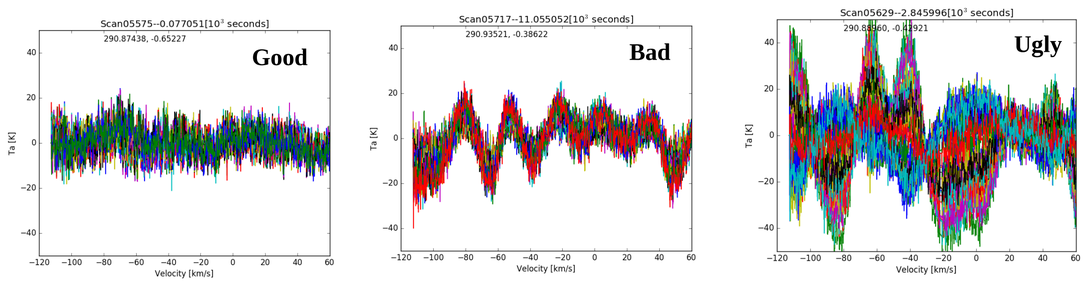

III. SOLUTIONS USING MACHINE LEARNING

- Sorting good and bad data using a clustering algorithm

  Clustering based on spectrum properties using DBSCAN (e.g., standing wave amplitude)

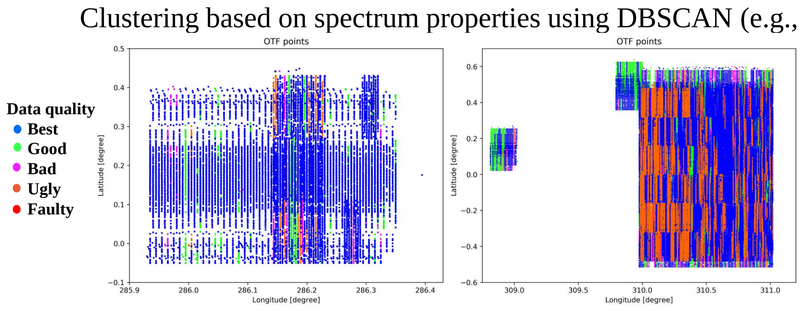

One dot denotes one spectrum.

Quality of data varies over observation time and modes.

- Defringe standing waves using deflation Independent Component Analysis (ICA)

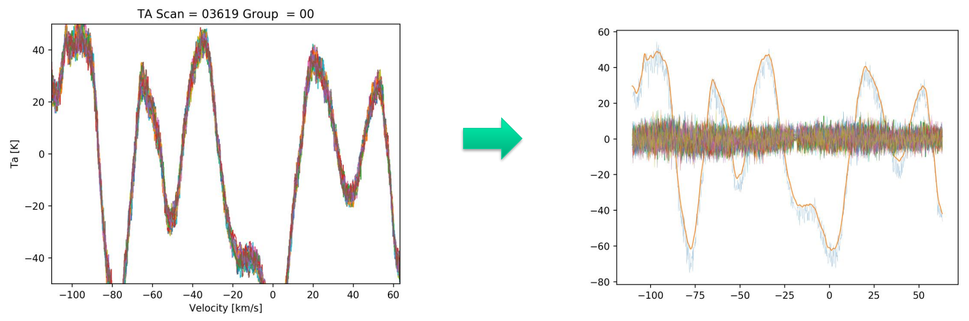

- A group of spectra having standing waves with a large amplitude
- First and second components of the deflation ICA are used to remove standing waves with a large amplitude.

- Baseline correction using parallel ICA

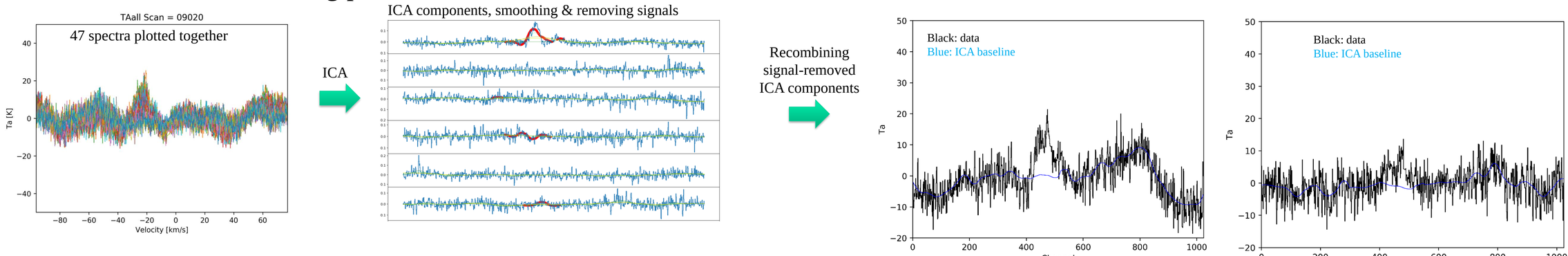

- Baseline of spectra is not stable and varies significantly over time.
- Conventional methods (polynomial baseline correction) require prior knowledge of emission line location, but it is hard to know when baseline is not stable.
- ICA is utilized to separate baseline and signal components and properly corrects baseline.

- Comparison between conventional methods and Machine Learning in Spectral maps

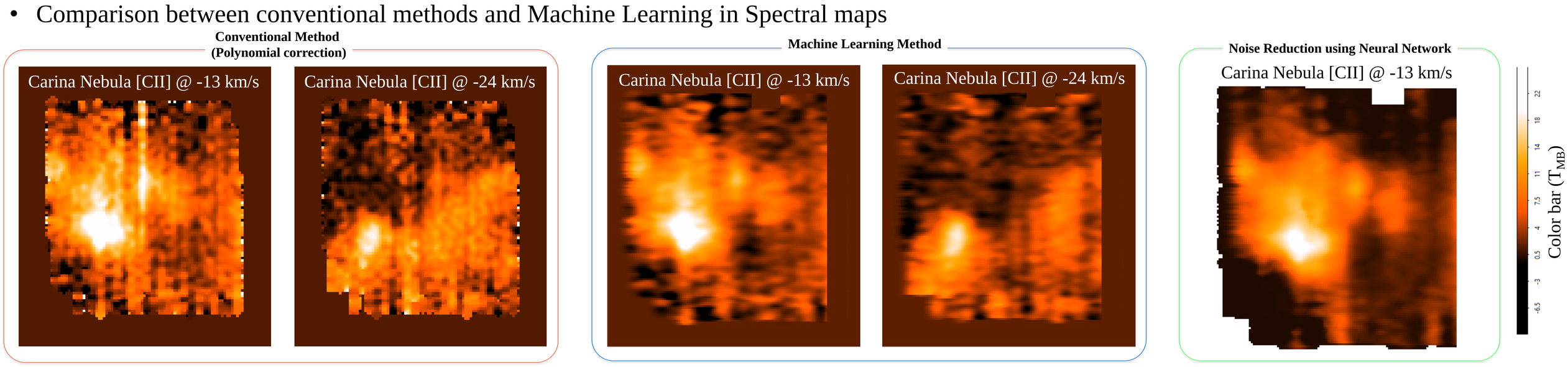

IV. IMPACT ON SCIENCE

- **Comparison of STO2 data to data from ISO satellite (comparison of integrated intensity)**
  - Conventional Method: deviation from ISO is ~70%
  - Machine learning method: deviation from ISO is ~20%
  - Noise reduced using CNN: deviation from ISO is ~17%
- **First science paper has been accepted by ApJ based on the data processed using the ML method** (arXiv:1903.09517)

V. FURTHER APPLICATIONS

- **The same algorithm can be used for other submillimeter and millimeter data**
- **Applicable to current and future facilities**

  Current: SOFIA GREAT instrument, DSN spectroscopy

  Future: GUSTO balloon, OST Decadal Flagship mission

National Aeronautics and Space Administration
Jet Propulsion Laboratory
California Institute of Technology
Pasadena, California

www.nasa.gov

Poster No. A-08

National Aeronautics and Space Administration

Modulation of The Cosmic Standard Ruler by Compensated Isocurvature Perturbations and Implications for Tensions

Author: Chen Heinrich (326)
Marcel Schmittfull, Olivier Doré (326)

What's compensated isocurvature perturbation?

Primordial perturbations in the Universe can be decomposed into two types: adiabatic and isocurvature, which can be further split for matter and radiation into an *effective* and *compensated* mode.

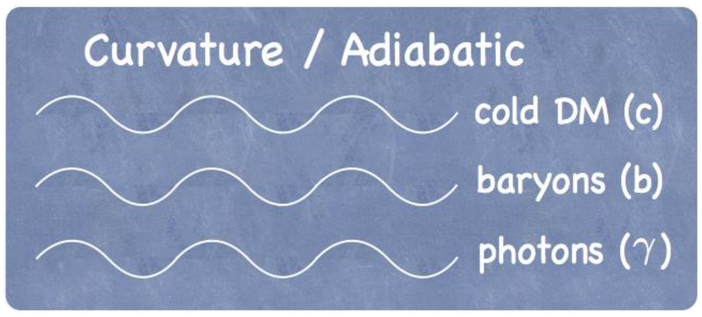

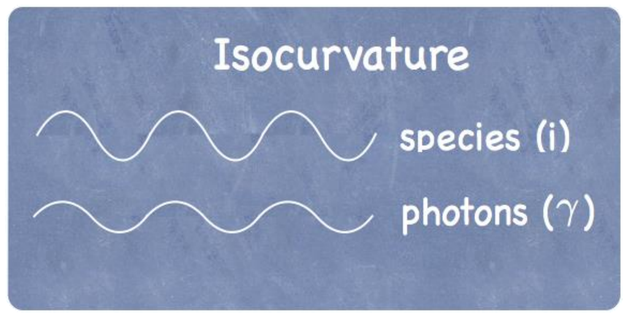

- **Effective mode**: well constrained (< 4% of adiabatic mode).

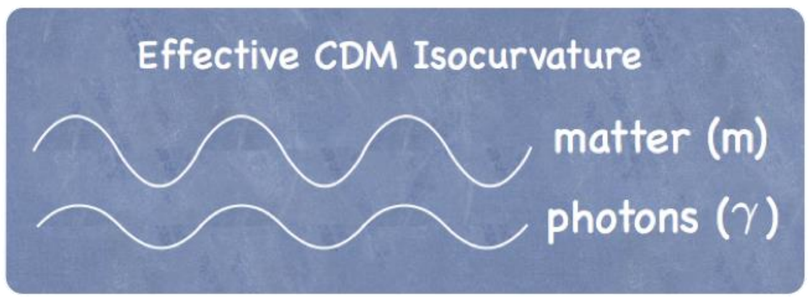

- **CIP mode**: baryon and dark matter (DM) have opposite fluctuations – *not well constrained*.

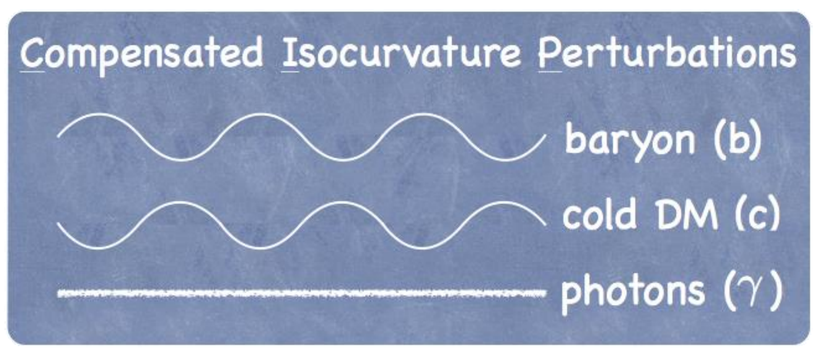

How do CIPs modulate our standard ruler?

- The spatial fluctuations of the baryon density causes an **inhomogeneous medium** for the sound waves to travel in the baryon-photon plasma.

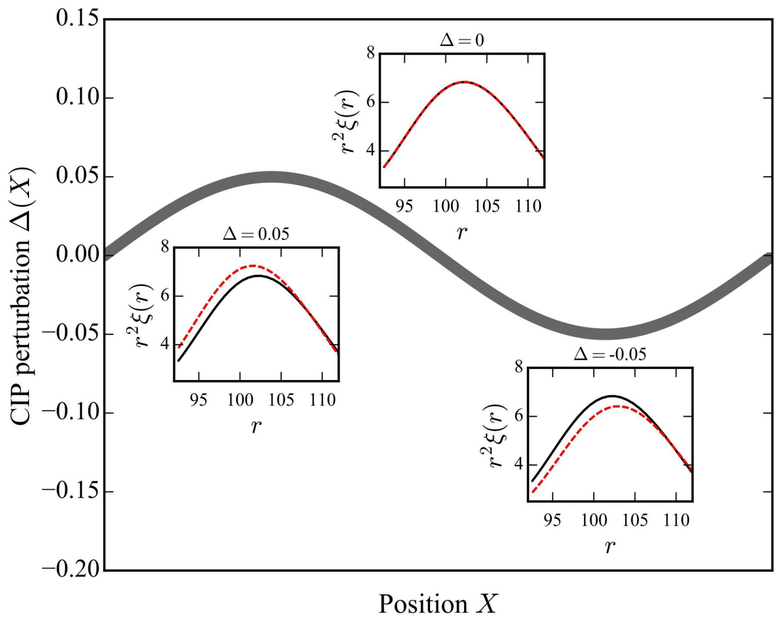

- As a result, the baryon acoustic oscillation (BAO) scale (a standard ruler we use in cosmology) appear shifted (peak location in the insets).

National Aeronautics and Space Administration
Jet Propulsion Laboratory
California Institute of Technology
Pasadena, California

www.nasa.gov

Measuring CIPs using BAO modulation

Method: 1) Divide galaxy survey into cells at $\boldsymbol{X}_i$; 2) measure the BAO scale α in each cell i; 3) use the CIP estimator: CIP($\boldsymbol{X}_i$) = C (α($\boldsymbol{X}_i$) - 1), C = cst. 4) Form auto power spectra (and cross-spectrum with galaxy density if looking for correlated CIPs).

Results: Future galaxy BAO surveys such as Euclid, or WFIRST in all-sky mode, can measure CIPs (correlated) with sensitiviy like WMAP.

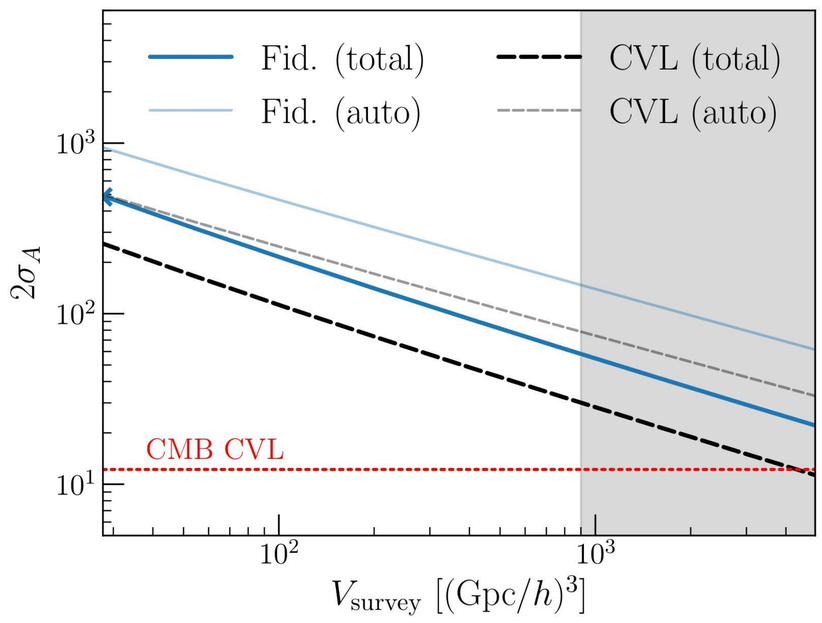

- Note: these results can be further improved with optimized estimator, multiple tracers, or 21cm BAO.

Cosmic-variance-limited surveys of emission-line galaxies up to z ~ 7 have sensitivity between current and next-stage CMB experiments.

The BAO method could provide a useful cross-check for CMB measurements of CIPs.

Implication for tensions in cosmology

- **Planck lensing anomaly**
  - CIP could be a possible explanation
  - Need cross-check from other probes

- **H0 tension**
  - The presence of CIP can bias our measurement of H0 assuming no CIPs.
  - CIP fluctuations at the level allowed by Planck power spectra measurements could relieve part of the H0 tension between BAO and supernovae measurements.

Poster No. A-10

National Aeronautics and Space Administration

Large-scale maps of the cosmic infrared background from *Planck*

Author: Daniel Lenz (3268)
Olivier Doré (3268)

Context

- The cosmic infrared background (CIB) **consists of all the unresolved infrared galaxies** in the Universe
- It is a powerful probe of the astrophysics of galaxies, the star formation history of the Universe, and the **connection between dark and luminous matter**
- The **key challenge** to obtain large-scale CIB maps is the **removal of foreground Galactic dust**

Conclusions

- We have obtained **new, large-scale CIB maps, extracted from the *Planck*** satellite data, published in Lenz, Doré, Lagache (2019, arxiv: 1905.00426)
- We used **Galactic neutral hydrogen from the HI4PI Survey** to model the Galactic dust foreground
- Our new maps agree well with previous ones, but **cover much larger areas and are subject to fewer systematics**
- The public maps have great legacy value, especially through **cross-correlations and by using them for CMB de-lensing**

Methods: Using HI to model foreground dust

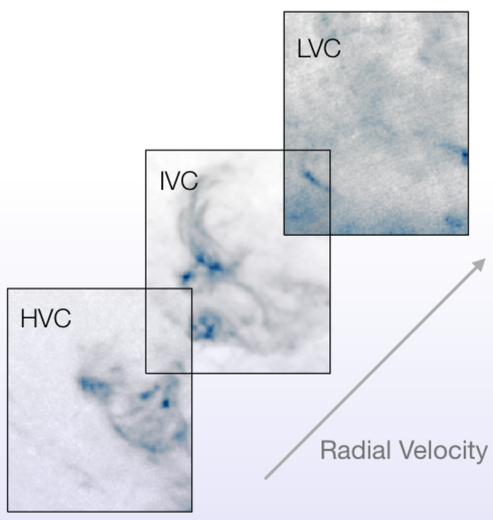

- The **standard approach** to modeling dust emission via HI is manually compute **HI column density maps for different gas phases**
- This requires a **manual separation** of the HI data cube
- Cannot account for complex structures or model large areas

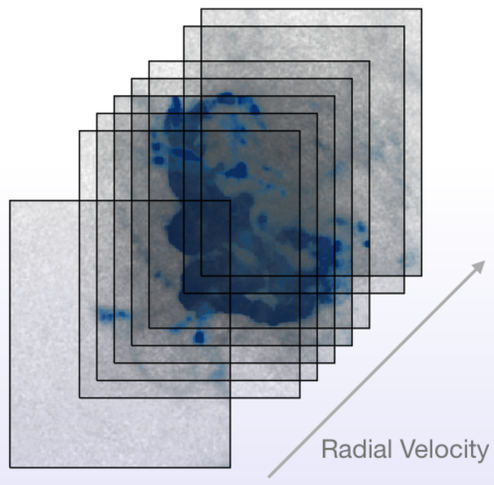

- Instead of accounting only for manually-chosen clouds, we **use each HI spectral channel**
- This allows to **automatically recognize all dust-emitting features**
- The results are **more robust, more accurate** and can be computed **unsupervised**

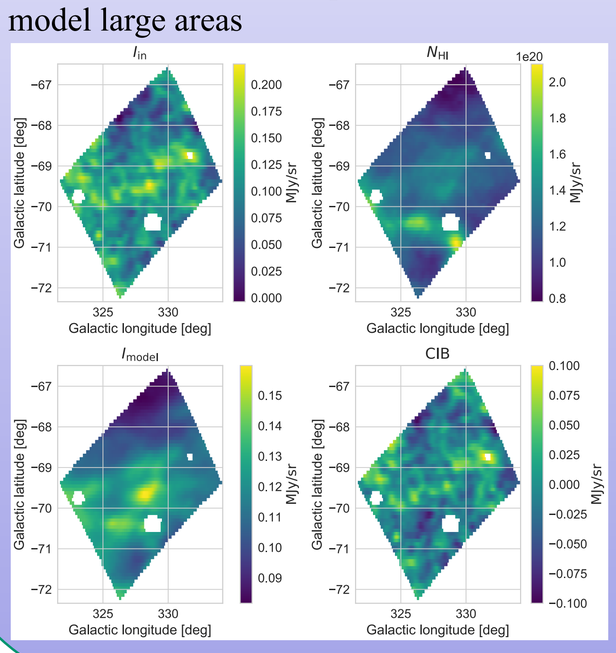

- Spatially, we **perform the component separation on small patches** at a time
- This **reflects variation in the dust-to-gas ratio**
- The main challenge is the ideal choice of spatial scales that **removes most dust, but preserves large-scale CIB fluctuations**

Results: Maps and angular power spectra

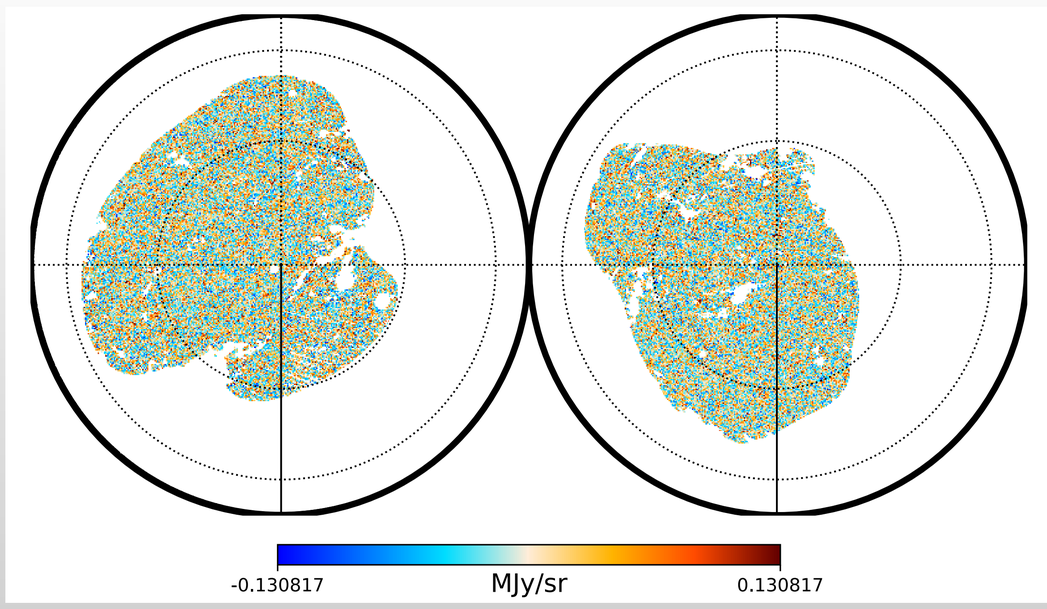

- We obtain CIB maps for **25% of the sky at the highest 3 *Planck* frequencies** (353 – 857 GHz)
- On smaller scales, we identify the high quality of the separation through the lack of dust emission for most parts of the sky
- We validate these products **through simulations, internal re-sampling, and comparisons with previous studies**

Total FIR intensity

Cleaned CIB image

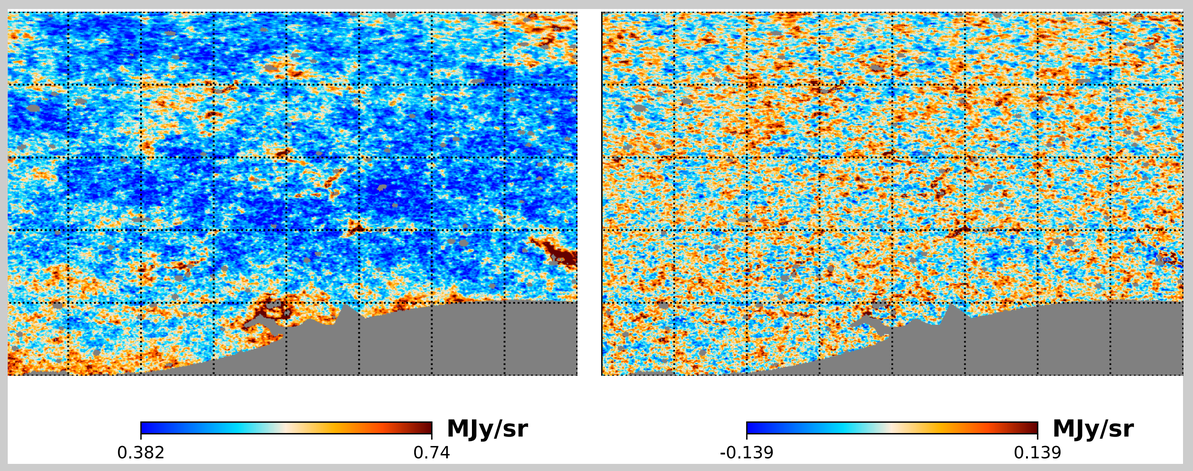

Outlook

- We will present a **detailed modeling of the resulting power spectra, resulting in better constraints on the cosmic star-formation history**.
- This can be used to **constrain e.g. the primordial non-Gaussianity f_{NL}**
- More sophisticated separation techniques and data sets
  - **Multi-frequency far-infrared data**
  - **Gaia data**
  - **Using deep learning to better model the complex ISM physics (JPL Data Science Pilot)**

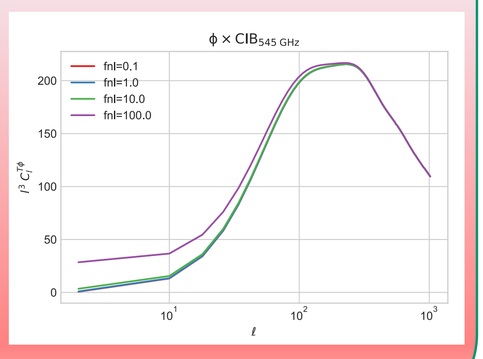

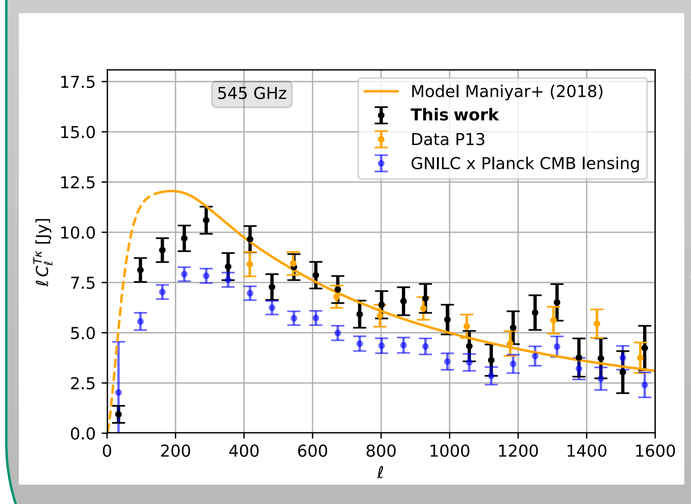

- The **cross-correlation with the *Planck* CMB lensing map** identifies the great overlap in the structures probes through the dusty CIB galaxies and the DM halos
- We obtain measurements on the largest scales, which have **great constraining power for parameters such as the non-Gaussianity f_{NL}**

National Aeronautics and Space Administration
Jet Propulsion Laboratory
California Institute of Technology
Pasadena, California

www.nasa.gov

Poster No. A-12

National Aeronautics and Space Administration

Measuring Galaxy Redshifts with Future Cosmology Surveys

Daniel Masters (Section 3268)

Collaborators: Daniel Stern (3266), Jason Rhodes (3200), Peter Capak (Caltech/SSC), Judy Cohen (Caltech), Bahram Mobasher (UC Riverside), Dave Sanders (IfA Hawaii)

Context

Understanding the "dark energy" causing the accelerating expansion of the universe is a fundamental goal of the upcoming ESA/NASA Euclid and NASA Wide Field Infrared Space Telescope (WFIRST) missions. A key cosmological probe both missions will use is *weak lensing*, which exploits the fact that the light of background galaxies is deflected by the gravity of intervening matter.

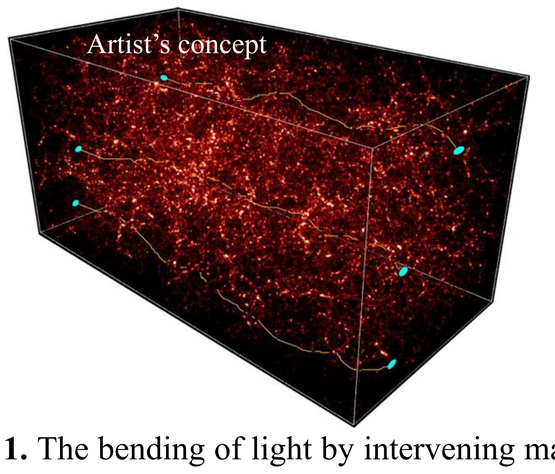

Figure 1. The bending of light by intervening matter as it propagates through the universe. This effect imprints a correlated shear in the shapes of galaxies that can be measured statistically in large imaging surveys.

Methodology

We developed a machine learning-based method to map the high-dimensional manifold of galaxy colors that Euclid and WFIRST will measure. The solution we found was the *self-organizing map* or SOM, which projects a high-dimensional data distribution to lower dimensions in a topologically ordered way. We applied this technique to photometry from deep extragalactic fields matched closely in depth and filters to the planned Euclid mission (Masters et al. 2015, 2019).

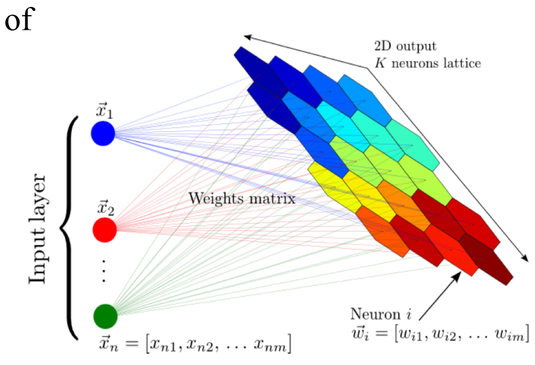

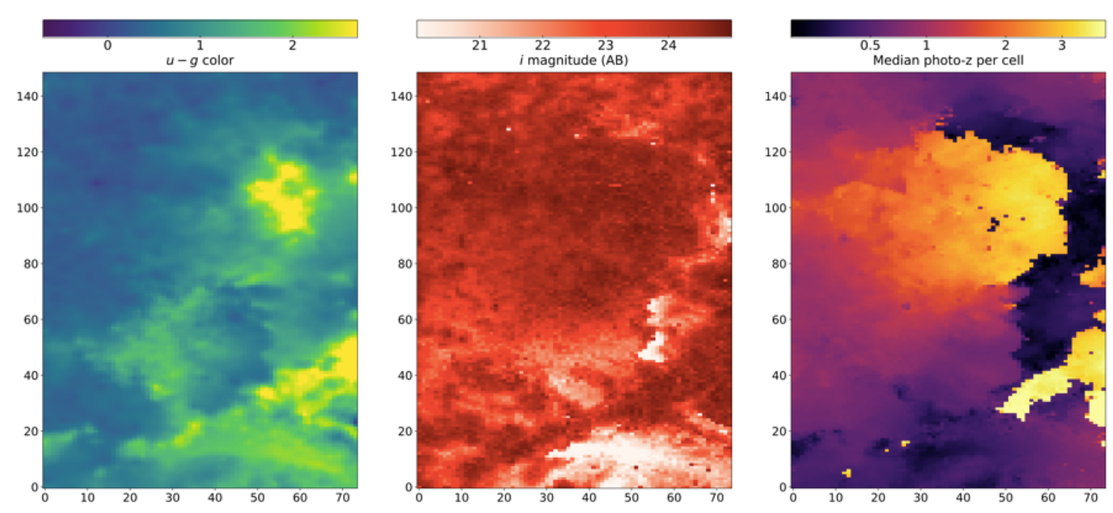

Figure 3. ***Left:*** Illustration of dimensionality reduction with the self-organizing map (from Carrasco Kind and Brunner 2014). ***Right:*** Different views of the SOM we developed from galaxy colors derived using deep field data (Masters et al. 2015, 2019). Each cell in the SOM represents a galaxy SED that shows up in the data with regularity. This map lets us identify where (in the color space relevant for photo-z estimation) we have sufficient spectroscopic data and where more constraints are needed.

The Redshift Measurement Problem

- To interpret the weak lensing signal, we must know the three-dimensional arrangement of the galaxies in the lensing sample. Thus we need galaxy *redshifts*, which are related to distance.
- We can only get high-precision spectroscopic redshifts for a small fraction of the $>10^9$ faint galaxies that will be imaged by these experiments.
- Therefore we must rely on *photometric redshift* (photo-z) estimates, which use imaging of galaxies in multiple filters to build a low-resolution view of the galaxy spectral energy distribution (SED).
- The requirements on the statistical accuracy of these photo-z estimates are extremely stringent; in particular they must be *highly unbiased.*

The Complete Calibration of the Color-Redshift Relation (C3R2) Survey

- A large, multi-institution, multi-instrument survey with the Keck telescopes to map the galaxy color-redshift relation in preparation for Euclid and WFIRST
- Joint effort of *all* Keck partners (Caltech, NASA, University of California, and University of Hawaii), with JPL leadership
- 44 nights allocated, ~4500 new spectroscopic redshifts critical to the calibration effort thus far (Masters et al. 2017, ApJ 841, 111; Masters et al. 2019 ApJ 877, 81)
- Data publicly available through Keck Observatory Archive (KOA)
- High visibility in community preparing for Stage IV cosmology missions

Principal Investigators:
Judith Cohen (Caltech) – 16 nights (DEIMOS, LRIS, MOSFIRE)
Daniel Stern (JPL) – 10 nights (DEIMOS, NASA Key Strategic Mission Support allocation)
Daniel Masters (JPL) – 16 nights (8 each LRIS/MOSFIRE, NASA Key Strategic Mission Support allocation)
Dave Sanders (IfA) – 6 nights (DEIMOS; upcoming H20 survey will contribute MOSFIRE/LRIS time)
Bahram Mobasher (UC Riverside) – 2.5 nights (DEIMOS)

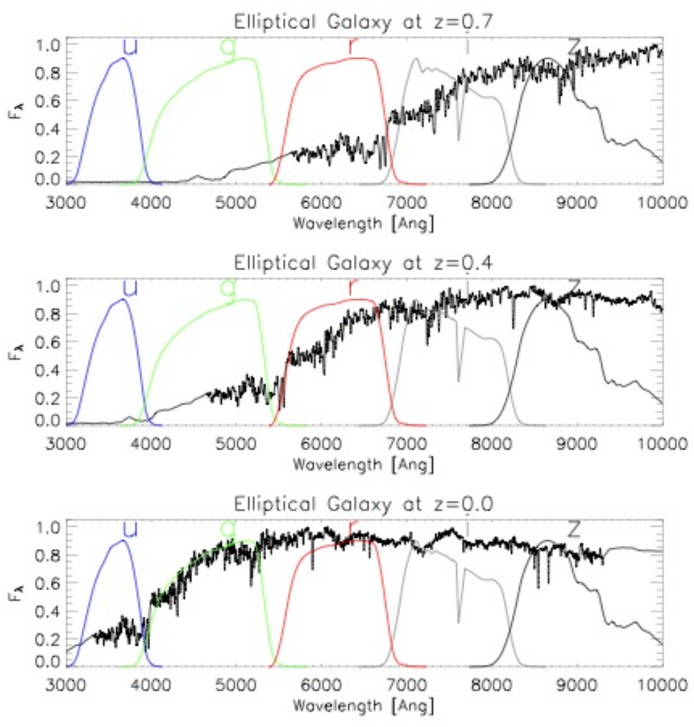

Figure 2. Illustration of photo-z estimation principle (from Padmanabhan et al. 2007). As a galaxy's spectrum is redshifted, it will display different fluxes and flux ratios in a given set of broad band imaging filters.

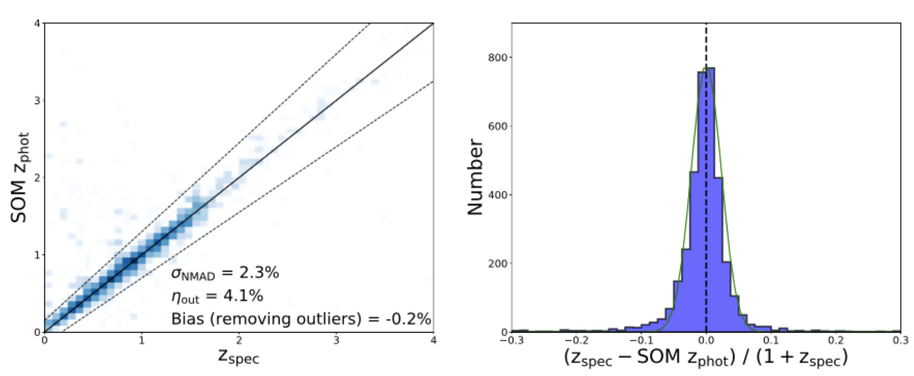

Figure 4. Results of the SOM-based calibration applied to the C3R2 spectroscopic sample of ~4500 galaxies obtained in the 2016A-2017A semesters. The method achieves unbiased redshift performance. We are continuing to test and refine the technique with both simulated and real data.

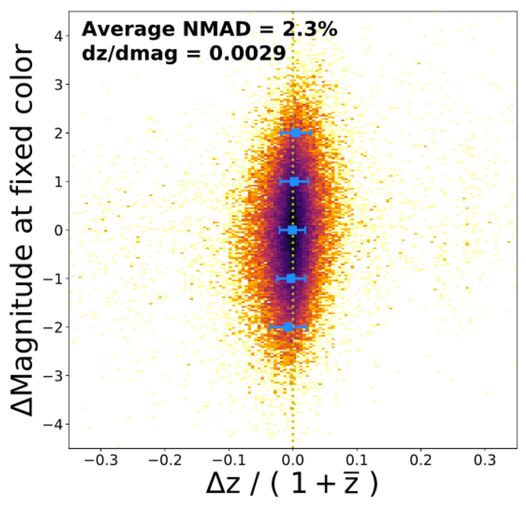

Figure 5. An important result from C3R2: at fixed Euclid/WFIRST color, the brightness of a galaxy carries little additional information about its redshift.

Conclusions

- We have developed a novel method to calibrate galaxy photometric redshifts for cosmology missions.
- Our method forms the basis of the C3R2 survey with the Keck telescopes to prepare for Euclid and WFIRST.
- Similar technique is now being used to explore estimation of galaxy properties beyond redshift.

Benefit to JPL

- The C3R2 survey is widely recognized in the cosmology community as *critical* to the success of the Euclid and WFIRST missions; JPL scientists play a leading role in this effort.

National Aeronautics and Space Administration
Jet Propulsion Laboratory
California Institute of Technology
Pasadena, California

www.nasa.gov

Poster No. A-13

Searching for Extended Dust Halos

Jacqueline McCleary (3268)
Eric Huff (3268)

National Aeronautics and Space Administration

Motivation

An analysis of millions of Sloan Digital Sky Survey galaxies revealed an unexpected **anomalous reddening extending up to 10 Mpc** from the galaxy centers. If this "extra" extinction is real, it has **profound implications** for models of the circumgalactic medium and for cosmological distance measurements. This result defies the predictions of hydrodynamic simulations of dust production and survival (Figure 1, right panel).

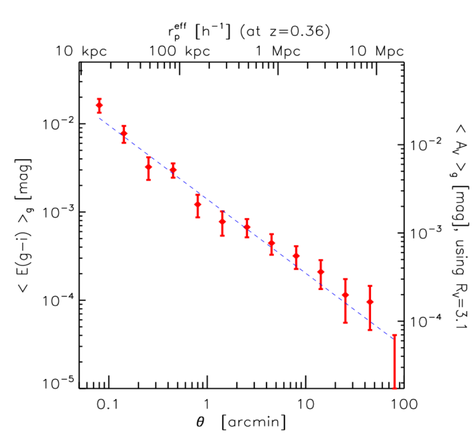

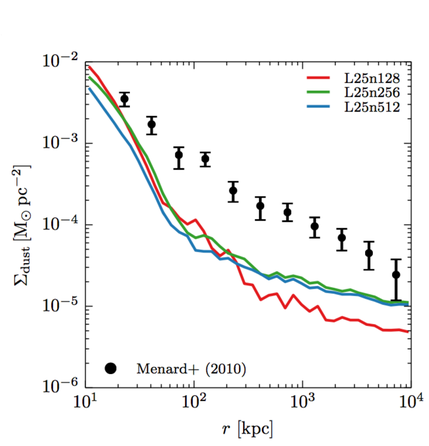

Figure 1. Left: Mean observer-frame reddening profile around i < 21 galaxies as a function of impact parameter. Taken from Ménard et al. (2010a). Right: Simulated dust surface density as a function of projected radius about galactic centers at z = 0.3. Taken from McKinnon et al. (2017).

IR Observations

- The differential dust extinction (A_v) between optical and IR bands is much larger than between optical bands alone.
- Accordingly, **we attempt to recreate Figure 1 with $\sim$ 10 foreground galaxy–background cluster pairs**
- We use J & H band imaging from the Widefield InfraRed Camera (WIRC) at Mt. Palomar Observatory, and optical data from the GALEX-Sloan-WISE Legacy Catalog

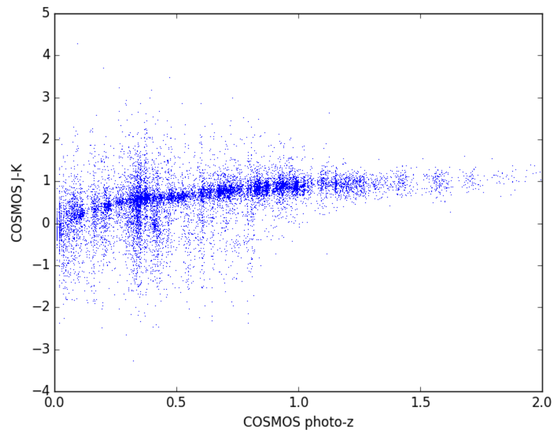

Figure 2. redMaPPer member galaxies form a very tight locus in color-magnitude space and are ideal "standard crayons" with which to search for anomalous reddening.

Extinction in Stacked DES Galaxies

- We also search for extended dust halos with a projected spatial correlation between 25,000 foreground galaxies and reddening of 670,000 background galaxies.
- Background sample ($0.2 < z < 1.3$) taken from the Dark Energy Survey (DES) Year 1 photo-z catalog
- Foreground galaxies taken from the WISExSCOS Photometric Redshift catalogue
- **We measure extinction with a maximum likelihood estimator for dust-induced reddening** by projecting the dust exctinction law $A_v(\lambda)$ for diffuse dust onto the color space of the DES galaxies.

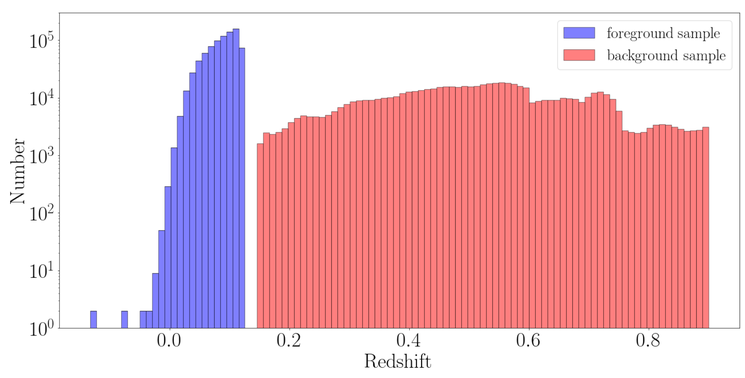

Figure 3. Foreground (WISExSCOS) and background (DES Y1) galaxy z distribution

Results from IR Observations

We measure the difference in cluster member galaxies between the SDSS g magnitude from the GSWLC catalog and the J-band magnitudes from WIRC observations.

These galaxy $g - J$ colors, which which carry information on the dust content, are plotted as a function of dustance from the cluster center.

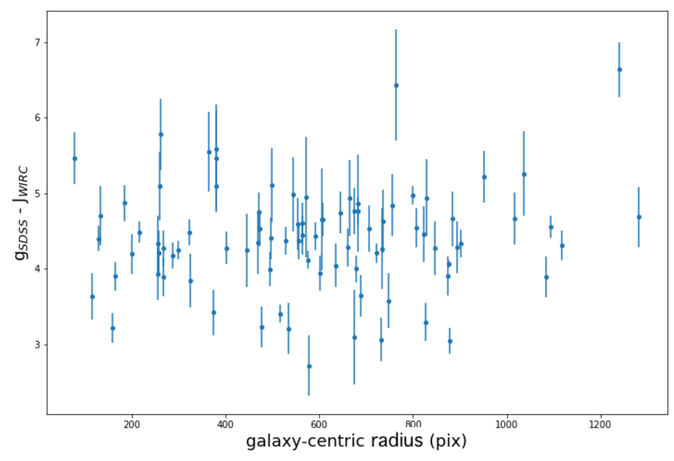

Figure 4. Sample differential extinction plot for a redMaPPer cluster behind a star-forming galaxy.

No trend is obvious in Figure 4, which is representative of our other WIRC imaging.

Results from DES analysis

The MLE for reddening is applied to each galaxy and correlated with the projected distance of foreground galaxies. The colors are converted to dust extinction A_v using the relation

$$\langle A_v \rangle(\theta) = 2.4 \times 10^{-3} (\frac{\theta}{1'})^{0.84}$$

The extinction is also computed along four "control" vectors. These vectors are perpendicular to the MLE in color space, and no reddening is expected.

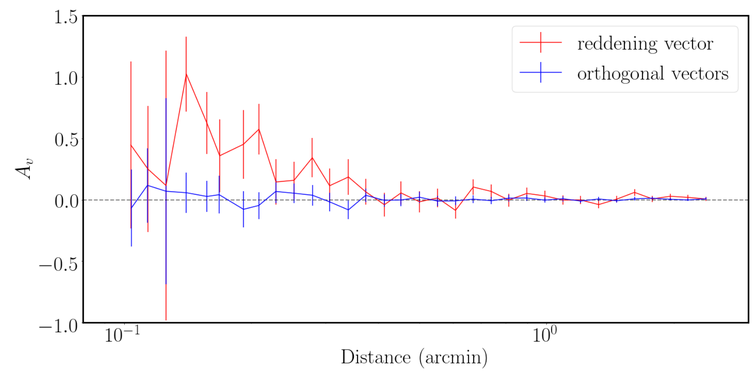

Figure 5. Extinction of background DES galaxies correlated with low-z foreground galaxies

.

A radially dependent extinction is clearly visible, and well above the reddening from the control vectors (plotted in blue).

Conclusions

Differential IR measurement on individual galaxy -- cluster pairs are inconclusive

- This is likely attributable to the fact that in J-band, dusty galaxies are not distinguishable in absorption from non-dusty galaxies. In addition, WIRC has strong non-linearity that makes precise photometry difficult.
- Analysis of stacked cluster/galaxy pairs will likely be required to make conclusive results, as well as comparison to random sample.

Stacked DES galaxy analysis shows strong extinction trend

- However, the exctinction is 100 times larger than expected from the literature.
- Likelihood testing against the random vector and searching for potential systematics are still needed to ensure the validity of our finding.

References

McKinnon, R., Torrey, P., Vogelsberger, M., Hayward, C. C., & Marinacci, F. 2017, MNRAS, 468, 1505
Ménard, B., Scranton, R., Fukugita, M.,& Richards, G. 2010, MNRAS, 405, 1025
Ménard, B., Kilbinger, M., & Scranton, R. 2010, MNRAS, 406, 1815.

National Aeronautics and Space Administration
Jet Propulsion Laboratory
California Institute of Technology
Pasadena, California
www.nasa.gov

Poster No. A-14

National Aeronautics and Space Administration

The Nature of Dark Matter with Strong Gravitational Lensing

Author: Anna Nierenberg 3268

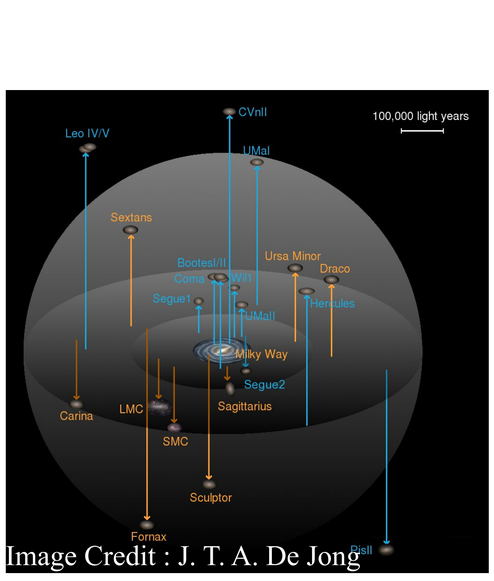

Image Credit : J. T. A. De Jong

2 keV/c² **Warm Dark Matter**

1 GeV/c² **Cold Dark Matter**

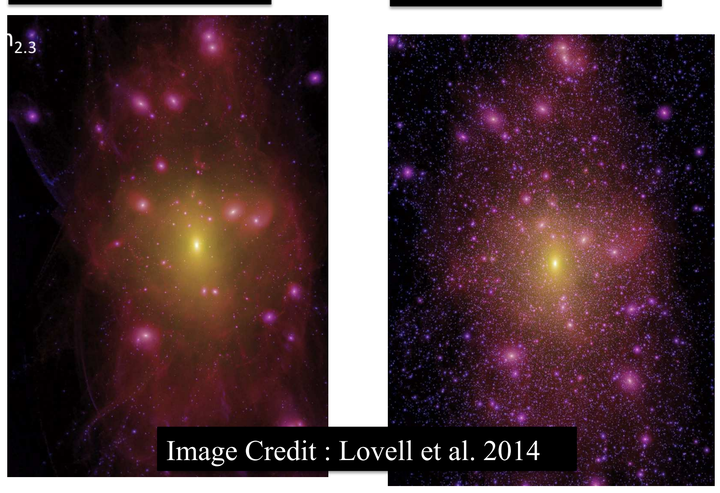

Image Credit : Lovell et al. 2014

What is dark matter?

The majority of matter in the Universe is believed to be collisionless particles which do not interact electromagnetically. Dark matter forms structures (halos), with galaxies in the centers. The **free streaming length** which controls the number of dark matter halos is a key open question in modern physics. If some halos do not contain observable galaxies we cannot tell the difference between a Warm and Cold Dark matter scenario with traditional methods.

Strong Gravitational Lensing

In a strong gravitational lens, a background source is multiply imaged with image positions and relative magnifications dependent on the mass distribution of the deflector.

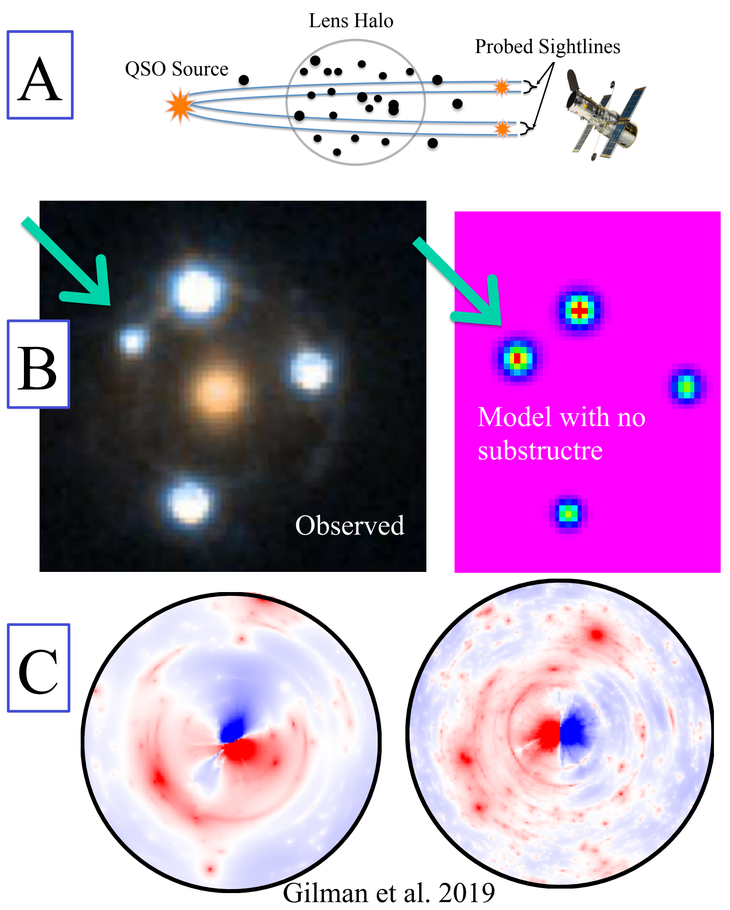

Gilman et al. 2019

Panel A. Small halos anywhere along the line of sight perturb the magnifications relative to their expected single deflector values.

Panel B shows a lens for which the magnifications have been distorted by small scale structure.

Panel C shows the lensing effect by substructure in a Warm (left) or Cold (right) dark matter Universe.

Panel D: The size of the lens source matters. If it is too small, there is also significant magnification due to stars in the main lens, as in the case of a quasar accretion disk (left). A large ~mas in projection source is needed to ensure small scale perturbations due to stars are averaged out (right). **For 2 decades this has limited the field to 7 radio loud quasar lenses**.

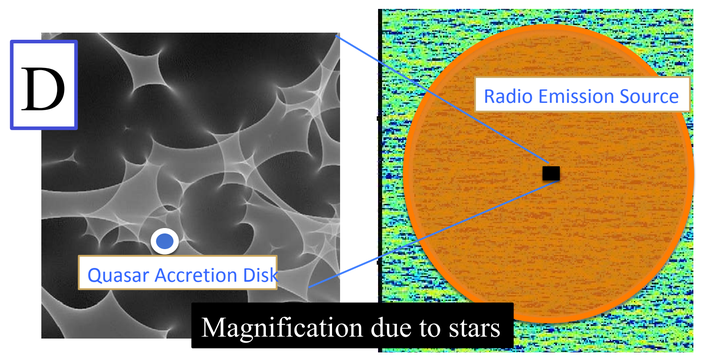

Gardsten et al. 2009 Stalevski et al 2009

A New Kind of Lens Source

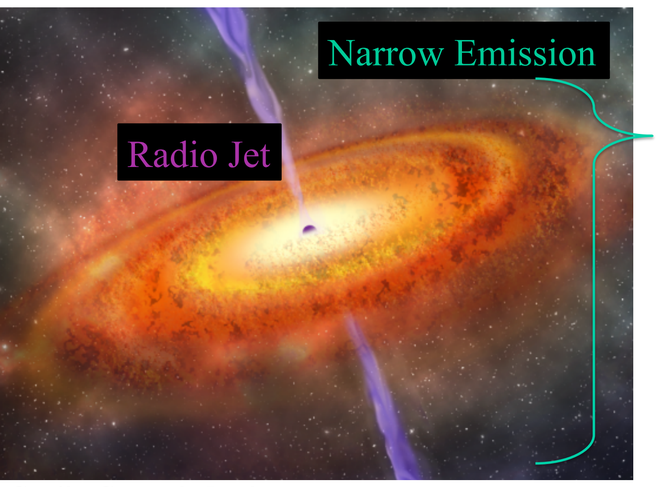

Credit: Carnegie Institute

Traditionally radio jets were the only source used to measure the halo mass function since its extended and not affected by microlensing. However radio jets are relatively rare. Many more quasars have significant narrow line emission. We use this narrow line emission as a lens source to enable us to more than double the number of systems which can be used for this measurement. (Moustakas and Metcalf 2003)

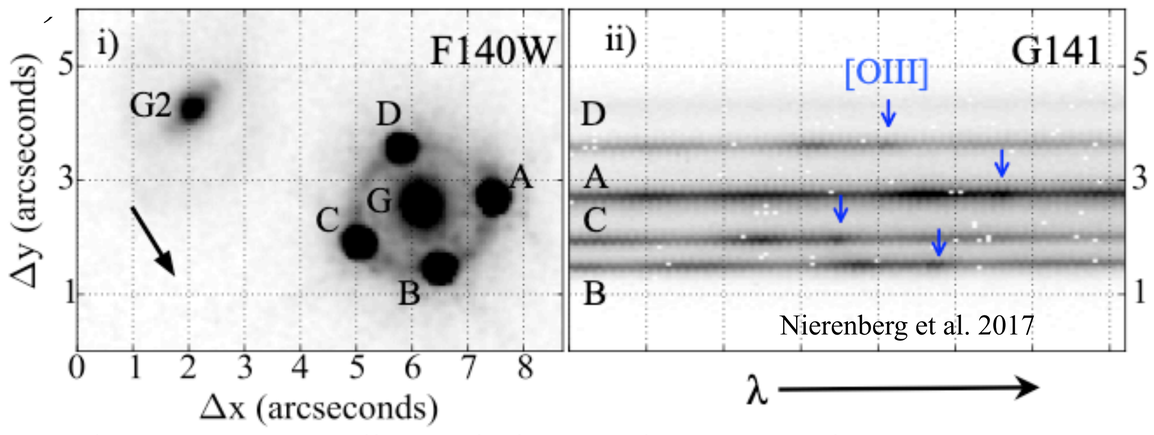

Nierenberg et al. 2017

In order to use narrow-line emission as a lens source, it's necessary to measure separate spectra in each lensed image, typically separated by less than 1 arcsecond spatially. This can be done using the HST grism. We have two HST programs to measure spatially resolved spectroscopy for a total of 15 strong gravitational lenses (GO-15177, GO-13732, PI Nierenberg). Combined with ground based adaptive optics measurements**, the new sample of lenses which can be used to measure the properties of dark matter on small scales is 22, triple the previous sample.**

The best constraint on the free-streaming length

With narrow-line lenses we more than triple the sample of systems which can do this measurement, enabling the tightest ever constraint on the dark matter free-streaming length. The current best limit is indicated by the yellow line from Lyα forest (Viel et al. 2013). We expect to get a constraint nearly this strong (purple band, fig. to right), with completely independent systematics. Future surveys such as Euclid/LSST will find hundreds of systems suitable for this method. (Oguri and Marshall 2010)

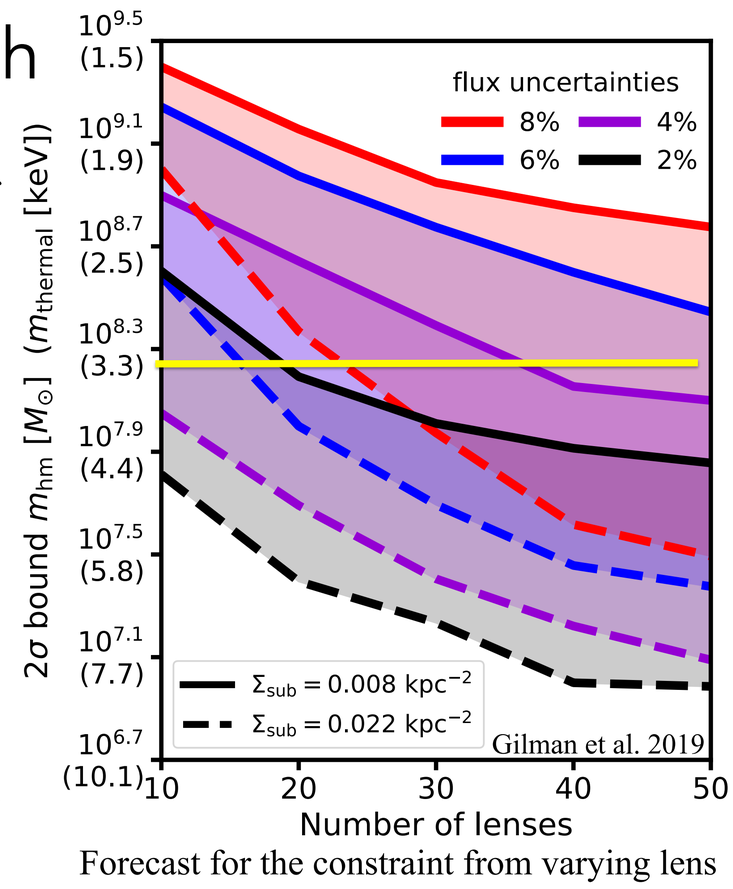

Forecast for the constraint from varying lens sample sizes and flux uncertainties. The bands indicate a range of model uncertainties.

National Aeronautics and Space Administration
Jet Propulsion Laboratory
California Institute of Technology
Pasadena, California

www.nasa.gov

Poster No. A-15

National Aeronautics and Space Administration

Meso-scale causes of high-latitude Ionospheric variability: What happened on the night of 2 March 2017?

Author: Dogacan Su Ozturk (335G)

Xing Meng (335G), Olga Verkhoglyadova (335G), Josh Semeter (BU), Roger Varney (SRI), Ashton Reimer (SRI)

1. Problem

Space Weather (geomagnetic storms and substorms) conditions can cause rapid and intense changes in the high-latitude ionosphere. The energy is dissipated on large (>500 km)**, meso- (100-500 km, <15 minutes),** and small-scales (<100 km).

Problem:

- Current forecasting efforts depend on global numerical models that **can't resolve the meso-scale structures** nor **use these fields as drivers**.
- Missing meso-scale electric field variability (temporal + spatial) causes **underestimation of energy input and dissipation** in the high-latitude Ionosphere.

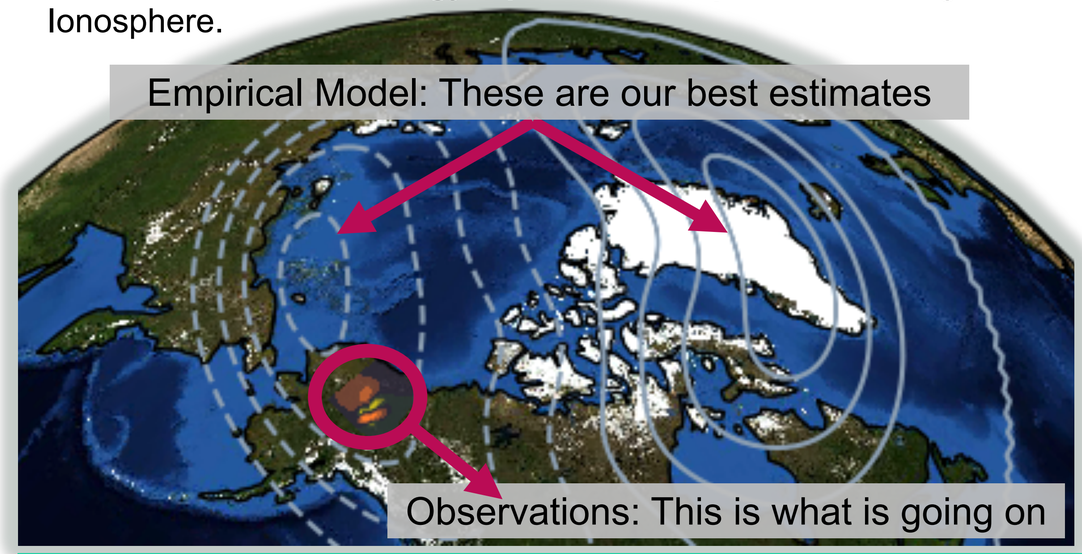

Goal: Incorporate dynamic drivers in a global model to improve our understanding of the high-latitude Ionospheric variability.

2. Data and Methodology

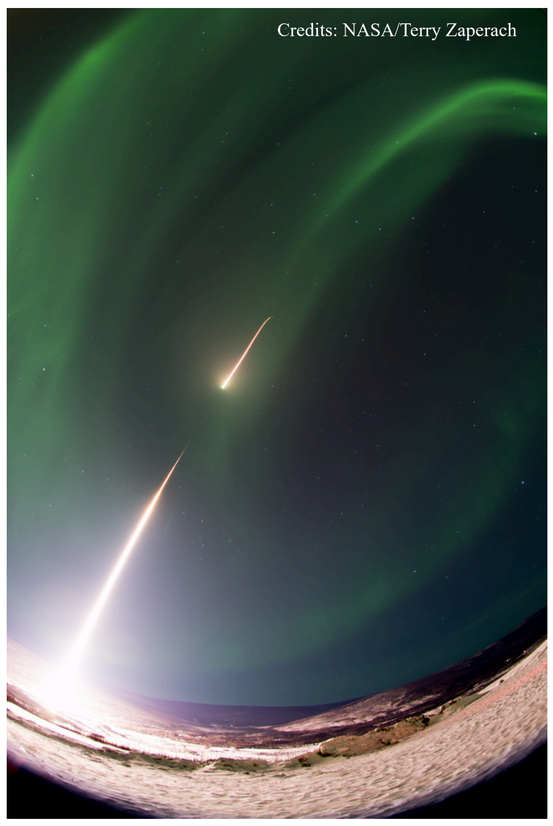

ISINGLASS sounding rocket experiment launched on **the night of 2nd March 2017**, into the auroral form to measure the plasma properties.

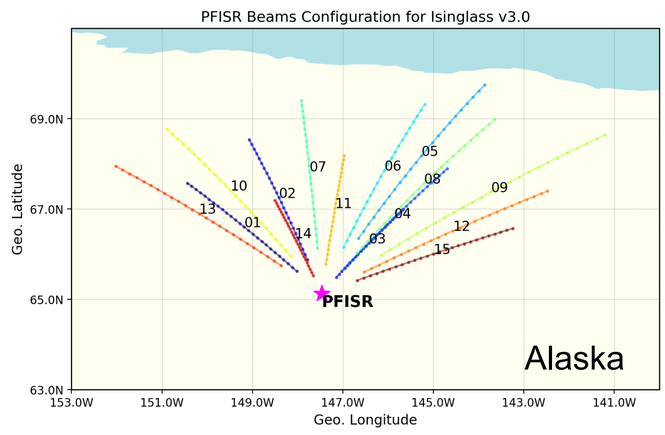

- Poker Flat Incoherent Scatter Radar (PFISR) operated on **a special multi-beam mode** to obtain **2D electric fields** and aid ISINGLASS mission.
- These high-resolution measurements can be used to **calculate electric field potentials** and **drive the global I-T model.**

Analyze meso-scale E field variability → Convert E fields to potentials (Total, Background, Variability) → Drive global I-T model to understand system response

3. Implementation of the Technique

I. Analyze Meso-scale Electric Field Variability

- The measured electric fields are decomposed into **"Background" and "Variability"** by subtracting 30 minute time averaged values.
- Then, the electric fields are integrated over a **desired grid**, to calculate electric potentials.
- To **preserve** the measured variability in both directions, we calculate **potential change in x and y**.

$$E_{total} = E_{background} + E_{variability}$$

$$\Delta\Phi_x = -\int_{x_1}^{x_2} E_x dx$$

$$\Delta\Phi_y = -\int_{y_1}^{y_2} E_y dy$$

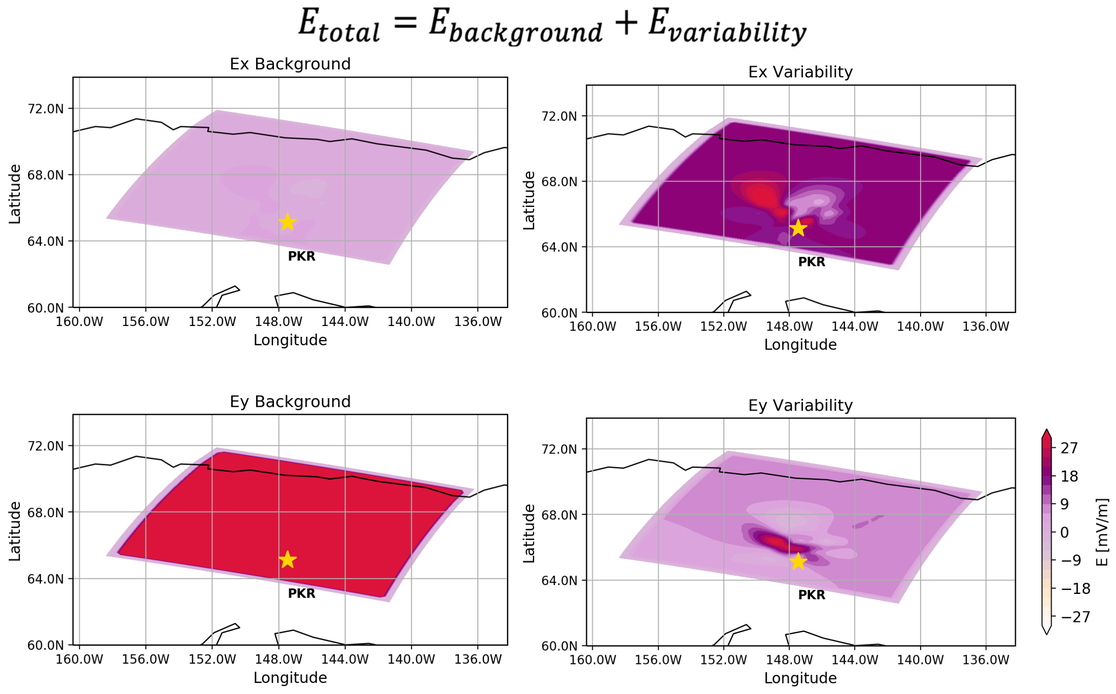

II. Convert Electric Fields to Global Drivers for the I-T Model

- Merge the calculated potential changes **with the empirical model** to drive the global I-T model.

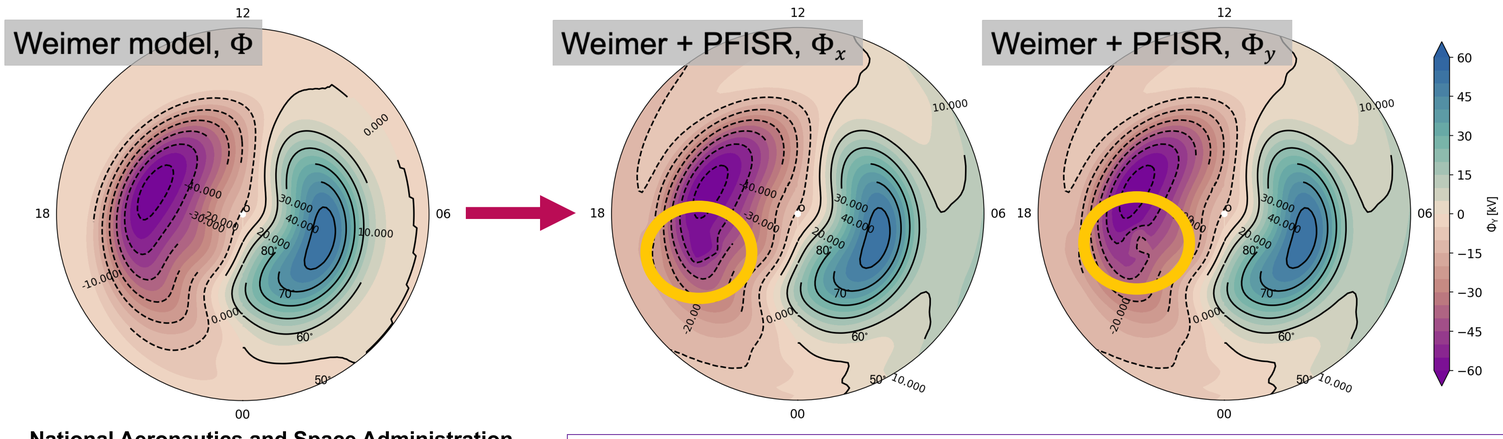

4. Conclusions

- We used 4 different inputs to drive the global I-T model, compared the results and calculated RMS errors along beams between 0626UT-0726UT.
- The results improved when the Variable, Background and Combined potentials were factored in.
- The measurement errors are comparable to the numerical errors.
- The biggest improvement was to the ion temperature, indicating the importance of ion convection mechanism for energy dissipation in I-T system.

	PFISR Beam-11		
Potentials	**RMSE Ne**	**RMSE Te**	**RMSE Ti**
Weimer Model	4.1E+10	998K	1764K
Calculated from E_{total}	3.7E+10	992K	1720K
Calculated from $E_{background}$	3.9E+10	991K	1723K
Calculated from $E_{variability}$	4.1E+10	996K	1745K
Errors in Measurements	4.2E+10	3054K	7167K

5. Summary and Future work

We developed a framework that can utilize **any 2D electric field measurement as input to run a global I-T model**. With this capability we are **now able to investigate the effects of meso-scale electric fields on the global energy budget** during active geomagnetic periods.

Our ongoing and **future work** include:

- Validation Studies: More events, different measurements
- Error and uncertainty quantification: Understanding how measurement and modeling errors propagate

National Aeronautics and Space Administration

Jet Propulsion Laboratory
California Institute of Technology
Pasadena, California

www.nasa.gov

Importance to NASA and JPL

This work enables the fundamental research outlined by the 2013 Heliophysics Decadal Survey's Key Science Goal 2 as well as operational capability that facilitates 2015 National Space Weather Action Plan's goals 4 and 5. The increased capability and understanding provided by this research is aligned with strategic directions of Section 335 Tracking Systems and Applications.

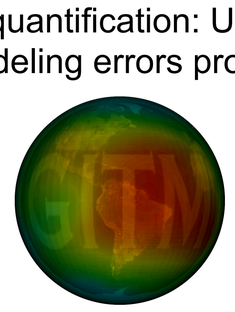

Poster no. A-16